Distal tephras along the SE European margin date powerful explosive eruptions from the Elbrus volcanic center (Greater Caucasus)

Vera Ponomareva[1], Maxim Portnyagin[2], Martin Danišík[3], Evgeny Konstantinov[4], Egor Zelenin[5], Nikolai Tkach[6], Folkmar Hauff[2], Axel K. Schmitt[7], Bjarne Friedrichs[7,8], Boris Romanyuk[9], Marcel Guillong[10], Christopher L. Kirkland[3,11], Kai Rankenburg[3], Samuel Müller[12], Dieter Garbe-Schönberg[12,13]

[1] Institute of Volcanology and Seismology, Piip Boulevard 9, Petropavlovsk-Kamchatsky, 683006, Russia

[2] GEOMAR Helmholtz Centre for Ocean Research Kiel, Wischhofstrasse 1-3, 24148 Kiel, Germany

[3] John de Laeter Centre, Curtin University, Perth, WA 6845, Australia

[4] Institute of Geography, Staromonetny Lane 29, Moscow, 119017 Russia

[5] Geological Institute, Pyzhevsky lane 7, Moscow, 119017, Russia

[6] Department of Oil-Gas Sedimentology and Marine Geology, Faculty of Geology, Lomonosov Moscow State University, Leninskie Gory 1a, 119991, Moscow, Russia

[7] Institute of Earth Sciences, Ruprecht-Karls-Universität Heidelberg, Im Neuenheimer Feld 236, D-69120, Heidelberg, Germany

[8] Department of Environment and Biodiversity, Paris-Lodron-Universität Salzburg, Hellbrunner Straße 34, A-5020 Salzburg, Austria

[9] Morinzhgeologiya Company, Rēznas 5-67, LV-1019, Riga, Latvia

[10] Department of Earth Sciences, ETH Zürich, Clausiusstrasse 25, 8092 Zürich, Switzerland

[11] Timescales of Mineral Systems Group, School of Earth and Planetary Sciences, Curtin University, Perth, WA 6102, Australia

[12] Institute of Geosciences, Kiel University, Ludewig-Meyn-Strasse 10, 24118 Kiel, Germany

[13] Department of Physics and Earth Sciences, Jacobs University Bremen, 28759 Bremen, Germany

***Corresponding author:**
Vera Ponomareva,
Institute of Volcanology and Seismology,
Piip Boulevard 9,
Petropavlovsk-Kamchatsky, 683006, Russia.
E-mail: vera.ponomareva1@gmail.com

Abstract

Knowledge of temporal patterns of past explosive eruptions is necessary to understand possible future eruptive behavior. However, volcanic records based on geological reconstructions remain incomplete. This inference is true not only for remote and sparsely populated areas like the Aleutian or Kurile-Kamchatka arcs, but also for Europe, where past large explosive events are continuously recognized in the geological record. Here we report the first age and geochemical data on the violent middle to late Pleistocene explosive eruptions from the Elbrus volcanic center (Greater Caucasus), which towers over the densely populated regions in southern Russia and Georgia. We attribute six disparate ash deposits found in the terrestrial and marine sediments along the SE European margin to the Elbrus volcanic center based on major and trace element compositions of individual shards of volcanic glass and radiogenic Sr-Nd-Pb isotope compositions of bulk tephra. We suggest that these deposits represent products of five different eruptions that were dispersed over distances of more than 150–560 km from their source. Three of four eruptions are dated at 522±36, 258±13, and 84.6±7.4 ka by a combined zircon U-Th-Pb and (U-Th)/He approach. One sample revealed an overdispersed spectrum of single crystal (U-Th)/He dates with an average of 176±40 ka. Zircon characteristics and statistical deconvolution of the geochronology data suggest that this sample contains zircon crystals from two different eruptions tentatively dated at 156.5±7.7 ka and 222.8±13 ka. These eruption ages represent the first recognition of a suite of large pumiceous eruptions from the Elbrus volcanic center postdating the previously known explosive activity, documented by ~800 ka old welded tuffs. These data also provide the first geochemical and geochronological characterization of both proximal and distal Elbrus tephra glasses and contribute to the global tephra database, permitting the identification of Elbrus tephras in distal terrestrial and marine paleoenvironmental archives and hence their use as paleoclimate and archaeological markers. We consider the significance of the identified tephras for paleoenvironmental research and

show their potential for tephrochronological studies in the East European Plain and adjacent areas.

1. Introduction

One of the prerequisites for predicting future giant eruptions is the understanding of the size and recurrence interval of past events and elucidation of the magma evolution of potentially hazardous volcanoes (e.g., Self and Gertisser, 2015). At the same time, the global record of large eruptions that is based mainly on geological evidence remains incomplete even for the last millennia (Deligne et al., 2010) and deteriorates deeper in time as many eruptions are yet to be identified (Rougier et al., 2016). This is true not only for remote and sparsely populated areas like the Aleutian or Kurile-Kamchatka arcs but also for Europe, where the eruptive record is frequently complemented by newly recognized large explosive events as, for example, the ~30 ka eruptions from Ciomadul in the Carpathians (Karátson et al., 2016) or the ~29 ka Masseria del Monte Tuff eruption from Campi Flegrei caldera (Albert et al., 2019), and extended back in time by the study of ash layers identified in long sedimentary archives (e.g. Giaccio et al., 2019; Leicher et al., 2021; Vakhrameeva et al., 2021).

Numerous findings of the Quaternary tephra in the East European Plain have been known since the early 1900s CE. However, until now, tephra from only one area -- a cluster of Paleolithic sites near Kostenki village (Don River; Fig. 1b), was geochemically characterized and linked to the widely recognized ~40 ka Campanian Ignimbrite eruption (Melekestsev et al. 1988; Pyle et al., 2006). Yet tens of other tephra deposits dispersed in the East European steppe from Penza and Tambov cities in the north to the Caucasus Mountains in the south remained poorly characterized, undated, and unlinked to their source volcanoes (e.g., Karlov 1957; Tsekhovskii et al. 1998; Gazeev et al. 2011; Fig. 1a). Although reconnaissance bulk chemical analyses have allowed the provisional attribution of few of the East European tephras to Elbrus or Kazbek volcanoes (Greater Caucasus), robust geochemical data and age control supporting these identifications were still missing (Lavrushin et al. 1998; Melekestsev et al., 2005; Gazeev et al., 2011). The lack of geochemical and age data on the East European tephras restricted their use as markers in expanding paleoenvironmental and archaeological research covering large territories from southeast European steppe to Transcaucasia (e.g., Golovanova et al., 2010; Doronicheva et al., 2019; Költringer et al., 2021; Lazarev et al., 2021; Yanina et al., 2021).

In this study, we geochemically characterize six distal tephra deposits found in terrestrial and marine sediments along the southeast European margin, from the middle Kuban River valley in the west to the Caspian Sea and lower Volga River valley in the east (Fig. 1; Tables 1 and S1). We apply a range of analytical techniques to determine major and trace elements of glass shards and radiogenic isotope composition of bulk tephra samples. Crystallization and eruption ages for four of these deposits are determined by combined U-Th-Pb and (U-Th)/He dating of zircon (a.k.a. "zircon double-dating" or "ZDD"; Danišík et al. 2017).

Five on-shore deposits have been reported earlier, while one from a marine core in the Caspian Sea is described here for the first time. Based on our new geochemistry data on distal and proximal tephras we suggest that they represent five eruptions from the Elbrus volcanic center (Greater Caucasus). We also report eruption ages for four of these eruptions and discuss the significance of the identified tephras for paleoenvironmental studies. Our data provide the first geochemical characterization of both proximal and distal Elbrus tephra glasses and contribute to the global tephra dataset, permitting the identification of Elbrus tephras in distal terrestrial and marine paleoenvironmental archives and their use as markers in paleoclimate and archaeological research.

2. Geological setting

2.1. Proximal volcanic record

The ~1200 km long mountain range of the Greater Caucasus runs from NW to SE separating the East European Plain and Transcaucasia (Fig. 1b). The range hosts two young large volcanic centers crowned with prominent cones of Elbrus (5642 m a.s.l.; Fig. 2a) and Kazbek (5047 m a.s.l.) volcanoes, which sit on the high-gradient alpine topography. In addition, a cluster of young monogenetic vents is located ~25 km SSW of Kazbek, on the Keli Highland (Fig. 1b). The two large Caucasian volcanoes tower over densely populated territories and pose hazard to adjacent regions of southern Russia and northern Georgia. The volcanoes are covered with perennial snow and glaciers, which may enhance the hazardous effect of future eruptions as those may cause melting of snow and glacial ice, resulting in lahars and snow-rock avalanches (e.g., Kraevaya, 1985; Bogatikov et al., 2001; Haeberli et al., 2004). Minor to moderate Holocene activity in the area was suggested for all three eruptive centers, but recent explosive eruptions occurred only at Elbrus and Keli (Bogatikov et al., 1998; Gazeev et al., 2011; Lebedev et al., 2010b; 2011b). The most recent eruption is believed to have occurred at Elbrus around 50 CE (Siebert et al., 2010), however, its products have not been firmly identified and the source of these data remains elusive.

Geochronology of volcanic activity in the Greater Caucasus is based predominantly on K-Ar dating of lavas (e.g., Lebedev et al., 2010a, b, 2011a, b, 2014, 2017, 2018; Kaigorodova et al., 2021). Explosive activity obtained less attention due to the complexity of proximal stratigraphy, where many pyroclastic units have been partly removed by erosion, obscured by younger volcanic products, or covered by snow and ice. Evidence of large explosive eruptions in the region dated so far include the Pliocene (~2.9 Ma) Chegem caldera ignimbrite (Lipman et al., 1993; Gazis et al., 1995; Bindeman et al., 2021) and welded ignimbrites near the Elbrus volcano (Gazeev and Gurbanov, 2004; Lebedev et al., 2011a; Chernyshev et al., 2014). While the Chegem eruption age is well constrained by $^{40}Ar/^{39}Ar$ and chemical abrasion isotopedilution thermal ionization mass spectrometry (CA-ID-TIMS) dating (Gazis et al., 1995; Bindeman et al., 2021), the ages of the welded ignimbrites around Elbrus are still disputed. For example, Gurbanov et al. (2004) provided zircon U-Pb sensitive high-resolution ion microprobe (SHRIMP) ages of 0.69–0.72 Ma for an ignimbrite unit sampled west of the Elbrus summit. Chernyshev et al. (2014) distinguished Pliocene (3.0–2.75 Ma) and early Pleistocene (0.84–0.7 Ma) ignimbrite units based on K-Ar dates on groundmass as well as on sanidine, biotite, and muscovite mono-mineral separates. Their dates for the upper, early Pleistocene unit are roughly similar to the age obtained by Gurbanov et al. (2004). In addition, Chernyshev et al. (2014) reported a single K-Ar date of 1.93±0.06 Ma for the groundmass from the rhyolitic "tuff lava" (welded tuff) northwest of Elbrus, which apparently represents another ignimbrite unit with respect to its age falling between the two earlier described units. The most recent study by Bindeman et al. (2021) reported laser ablation - inductively coupled plasma - mass spectrometry (LA-ICP-MS) zircon U-Pb ages of ~2 Ma for both older and younger ignimbrite units. These dates are at odds with the earlier suggested ages for both units but are similar to the age estimated for the "tuff lava" reported by Chernyshev et al. (2014). The existing complexity in the geochronological datasets may have arisen from the difficulties of field identification and correlation of different units in proximal outcrops; at the same time, such complexity demonstrates a need for reliable geochronology of explosive eruptions in this area.

Thick pumiceous deposits overlying welded ignimbrites northeast and west of Elbrus point to younger explosive eruptions. However, those deposits have never been dated and were characterized by only a few XRF analyses on bulk samples (e.g., Kraevaya et al., 1985; Melekestsev et al., 2005; Gazeev et al., 2011). Consequently, a large part of the history of explosive activity in the area remains unknown. The K-Ar ages of lava flows, however, suggest that the post-ignimbrite activity from the Elbrus volcanic center occurred during three phases at 225–170 ka, 110–70 ka, and within the last 30 ka (Lebedev et al., 2006, 2010b; Chernyshev et al., 2014).

2.2. Distal tephra record

Many findings of Quaternary tephra were described north and south of the Greater Caucasus Range – in the southern part of the East European Plain and in Transcaucasia (e.g., Karlov 1957; Tsekhovskii et al. 1998; Gazeev et al. 2011; Wolf et al., 2016; Lazarev et al., 2021). North of the Greater Caucasus, tephras were found in thick loess-paleosol sequences (LPS) (Melekestsev et al., 1988, 2005; Bolikhovskaya, 1995), in caves (Hidjrati, 2003; Golovanova et al., 2010; Doronicheva et al., 2019), and in sediments of a Caspian marine transgression (Lavrushin et al., 1998). To the south, tephra layers were described in various deposits including, again, sediments of the Caspian marine transgressions, paleolakes, and caves (e.g., Ganzei, 2003; Gazeev et al., 2011; Van Baak et al., 2019; Lazarev et al., 2021). However, only very few of these studies offer major element data on tephra glasses (e.g., Pyle et al., 2006; Cullen et al., 2021; Sherriff et al., 2021) while no single-shard trace element data for glasses are available. Until now, only one tephra in the area north of the Greater Caucasus was geochemically linked to its source – the widespread ~40 ka Campanian Ignimbrite ash found in Paleolithic sites around Kostenki village (Fig. 1b; Melekestsev et al. 1988; Pyle et al., 2006).

3. Samples and methods

3.1. Distal tephras

For our study, we used distal tephra samples from five on-shore sites and one marine core located along the southeastern European margin (Fig. 1; Tables 1 and S1; Supplementary Text). Of those, five terrestrial tephra deposits have been described earlier (Karlov, 1957; Lavrushin et al., 1998; Tsekhovskii et al., 1998; Melekestsev et al., 2005; Gazeev et al., 2011) and a sample from the marine core is described here for the first time. In terms of grain size, tephras range from small pumice lapilli to very fine ash. Based on the positions of the tephra sites and tephra thicknesses, the Greater Caucasus Range volcanoes appear as the most plausible sources.

Two tephras (labeled TMG and OTK), found near Temizhbekskaia and Otkaznoe villages, respectively, are deposited within loess-paleosol sequences (Fig. 2b-e; Melekestsev et al., 2005; Bolikhovskaya, 1995). The TMG tephra deposit was identified as a 20–80 cm thick and several meters long lens, composed of light-gray to white fine ash (Fig. 2d, e) (Melekestsev et al., 2005). The tephra is layered, with distinct signs of fluvial redeposition into a gully; however, as it is composed mostly of clean ash, the redeposition likely took place almost simultaneously with the tephra fall. The average thickness of the individual sublayers is ~5 cm, which was used as a best estimate of primary ash thickness in the volume calculations.

The OTK tephra deposit forms large lenses in the bluffs at the eastern bank of the Otkaznensky reservoir. The 17–20 m long and up to 70 cm thick main lens fills the gully and is overlain with a loess-soil package including a modern soil and two paleosol horizons (Fig. 2b, c). The lower tephra sublayer is ~30 cm thick massive pumiceous sand. We interpret this part of the tephra layer as a primary fall deposit. The upper 40 cm of the lens is a thinly layered gray ash. This part obviously was redeposited within the depression. In 1980s, ash pods were described by Viktor Udartsev in the same loess-paleosol sequence (LPS) ~700 m to the north-east (Bolikhovskaya, 1995). As these old samples are no more available it is not clear whether this was the same ash as our OTK.

Two tephras (labeled SARM and VL) were visibly recognized in the marine deposits. SARM tephra was taken from a Caspian Sea sediment core, and VL tephra - from ancient marine deposits in the lower reaches of the Volga River (Lavrushin et al., 1998). The SARM tephra deposit forms a homogeneous and pristine 75 cm thick layer composed of fine ash. As no further information on the enclosing deposits is available, we cannot evaluate whether the whole ash layer represents an original 75 cm thick fall unit or whether submarine sediment transit increased the layer thickness at the site. The VL tephra deposit was found as an up to 70 cm thick and at least 100 m long lens of very fine ash within the deposits of the paleo-Volga delta slope (Lavrushin et al., 1998). The tephra lacks layering or grading but its variable thickness and lens-like character suggest some redeposition.

The TSK tephra deposit found in South Ossetia is a remarkably laminated ash with a visible thickness of >10 m (bottom unexposed), which suggests its redeposition into a paleolake basin (Gazeev et al., 2011; Figs. 1b; 2f,g). The BU tephra deposit was identified near Buynaksk town (Dagestan) and initially described as a 1.5 m thick layer on the top of alluvial deposits (Matsapulin et al., 2008). Our revision of this site in 2022 allowed assessing the thickness of non-disturbed primary ash layer at ~15 cm.

3.2. Proximal samples

In order to characterize proximal Greater Caucasus Range tephras with a clear spatial link to their origins, we collected several pumice samples from the vicinity of Elbrus volcano and Keli monogenetic centers (Table S1; Supplementary Text). No large proximal tephras are known for the other prominent volcano, Kazbek (Lebedev et al., 2018).

For the Elbrus eruptive center, proximal pumice samples were taken from two sites near the Zhilysu (Jily-su) mineral springs (~12 km NE from Elbrus), and from a site at the Baksan River (~46 km ENE from Elbrus) (Supplementary Text, Fig. S1). Both Zhilysu sites exhibit thick stratified pumice packages (Figs. S2 and S3). The first site (Elbrus-5) exposes layered pumice fall deposits without distinct signs of redeposition while the second site (Elbrus-6) contains layers of cross-bedded pumiceous material likely reworked by the river. The site at the Baksan River terrace exhibits a stratified package of redeposited pumiceous sands and silts (Fig. S4). Samples from Keli Highland were collected from lake deposits near the vents.

3.3. Methods

We applied a range of analytical techniques to determine the age of investigated tephras and characterize their chemical composition. Zircon crystals from SARM, TMG, OTK, and proximal Elbrus-5-5 tephras were dated using the ZDD approach (Danišík et al. 2017). Geochemical studies included in situ micro-analyses of individual volcanic glass shards by electron probe microanalysis (EPMA) and laser ablation - inductively coupled plasma - mass spectrometry (LA-ICP-MS) as well as determination of radiogenic Sr, Nd, and Pb isotope ratios in bulk samples by thermal ionization mass-spectrometry (TIMS). Analytical details of each method can be found in Supplementary Text and the instrumentation used is summarized below.

Zircon crystals from samples SARM, TMG, and OTK were dated by U-Th disequilibrium or U-Pb methods (if crystals were in secular equilibrium) using Secondary Ion Mass Spectrometry (SIMS) in the Heidelberg Ion probe (HIP) Laboratory at the Institute of Geosciences, Heidelberg University (Germany). Zircon from sample Elbrus-5-5 was U-Pb dated by LA-ICP-MS using a 193 nm ASI Resolution ArF excimer laser connected to a Nu Plasma II multi-collector (MC) ICP-MS at Geohistory Facility in the JdLC, Curtin University, and U-Th disequilibrium dated using a 193 nm ASI Resolution ArF excimer laser connected to a Thermo Element XR™ High Resolution sector field ICP-MS at ETH Zürich (Switzerland). After the SIMS and LA-ICP-MS analyses, zircon crystals were (U-Th)/He dated in the JdLC Western Australia Thermochronology Hub (WATCH) facility (Curtin University) using Alphachron II instrument and an Element XR™ High Resolution ICP-MS.

EPMA data were obtained at the GEOMAR Helmholz Centre for Ocean Research Kiel (Germany) using JEOL JXA 8200 wavelength dispersive electron microprobe. The analytical conditions for glasses were 15 kV accelerating voltage, 6 nA current and 5 µm electron beam size. LA-ICP-MS analyses of major and trace elements were conducted at the Institute of Geosciences at Kiel University (Kiel, Germany) using a Coherent GeoLas HD ArF 193 nm excimer laser system coupled with single quadrupole Agilent 7900 ICP-MS or with tandem-quadrupole Agilent 8900 ICP-MS/MS (beginning from early 2021). The analyses were performed using a laser spot size of 24 µm, pulse frequency of 10 Hz, and fluence of 5 J cm^{-1}, and included all major elements. Detailed description of the analytical setup, procedures of data quantification, and quality control for EMPA and LA-ICP-MS analyses are provided by Portnyagin et al. (2020). Sr-Nd-Pb isotope ratios were determined at the GEOMAR Helmholtz Centre for Ocean Research Kiel (Germany) on a TRITON Plus TIMS following the procedures outlined in Hauff et al. (2021) and references therein.

A workflow of tephra volumes and eruption magnitudes estimation began with the assessment of primary tephra thickness in outcrops. Then a minimum convex envelope was drawn for locations of tephra sites and the source volcano, serving as the most conservative model of an isopach. Finally, an area of isopach and its thickness were accounted in a single-isopach minimum estimate of ash-fall volume, proposed by Legros (2000) and further recalculated to eruption magnitude (Pyle et al., 1995) using tephra density of 800 kg/m^3. The workflow uses conservative estimations on every step, and thus any further tephra findings will likely increase our initial estimates.

4. Results and Discussion

4. 1. Tephra eruption ages

Zircon crystals from distal SARM, TMG, OTK and proximal Elbrus-5-5 tephras were dated by using a combined U-Th-Pb and (U-Th)/He dating approach (a.k.a. "zircon double-dating" or "ZDD"; Danišík et al. 2017) to constrain the eruption age. ZDD results are summarized in Table 1 and graphically presented in Fig. 3. Details of the method are provided in the Supplementary Text and the complete data set is in Supplementary Tables S2-12.

Alpha-ejection and disequilibrium corrected (U-Th)/He dates for samples OTK and TMG individually form single homogeneous populations and display MSWD values of 1.4 (n=12) and 1.9 (n=9), respectively. Such age spectra are typical for quickly cooled samples and therefore the corresponding weighted mean values of 522±36 ka and 258±13 ka (the uncertainties correspond to 95% confidence intervals) are interpreted as eruption ages for samples OTK and TMG, respectively.

Sample SARM-4 revealed more dispersed alpha-ejection and disequilibrium corrected single grain (U-Th)/He dates with an MSWD value of 4.2 (n=20). We note that such increased dispersion is not uncommon in ZDD datasets (e.g., Danišík et al. 2020) as it may reflect our limited ability to quantify the uncertainties and/or our simplified assumptions regarding the alpha-ejection correction (e.g., homogeneity of parent nuclides, or idealized grain geometry). The weighted mean value of 84.6±7.4 ka is therefore considered our best estimate of the eruption age for sample SARM.

Sample Elbrus-5-5, which consists of pumice lapilli and coarse sand, contains a mixture of zircon crystals of different shape and color typical for a detrital sample. An effort was made to date the different zircon types using LA-ICP-MS. Resulting U-Th disequilibrium and U-Pb ages (n=82) range from 171^{+21}_{-18} ka to 2.2±0.03 Ma (1σ uncertainties), confirming the dated zircon crystals originated from different sources. The TuffZirc age algorithm (Ludwig and Mundil, 2002) was applied to the obtained U-Th-Pb data in order to identify a statistically coherent youngest age component and yielded an age of 296^{+19}_{-28} ka (95% confidence interval) based on a group of 59 ages (Supplementary Tables S17). Given that the U-Th-Pb data record zircon crystallization, the TuffZirc age of 296^{+19}_{-28} ka age provides the maximum eruption age for sample Elbrus-5-5. Alpha-ejection and disequilibrium corrected (U-Th)/He dates, which were obtained preferentially on the zircon grains with youngest crystallization ages (i.e., closest to the youngest eruption event), form a broad over-dispersed population (MSWD=8; n=20) with single grain (U-Th)/He dates ranging from 117±24 to 250±16 ka (1σ uncertainties).

As in the case of sample SARM-4 discussed above, it is possible that this scatter of ages could stem from simplified assumptions regarding alpha-ejection correction and its uncertainties. Therefore, the measured dataset may be represented by a weighted mean of 176±40 ka (the uncertainty in this case is one standard deviation to honor the fact that the population is over-dispersed and therefore the 95% confidence interval can be misleading), which can be treated as a conservative estimate of the eruption age for sample Elbrus-5-5. However, this broad age range may suggest that despite our effort to date the youngest crystals, the (U-Th)/He dated zircons rather represent a mixture of crystals erupted at somewhat different times. Deconvolution of the dataset using the mixture modelling approach of Sambridge and Compston (1994) reveals two components: 157±8 ka and 223±13 ka (2σ uncertainties), suggesting that the double-dated zircon crystals from sample Elbrus-5-5 may have been erupted in two volcanic events, one at 156.5±7.7 ka and the other at 222.8±13 ka. At the same time, as the proximal pumices from site Elbrus-5 are chemically quite homogeneous they would seem to represent a single eruption. These facts suggest that, with the currently available data the age of sample Elbrus-5-5 cannot be conclusively resolved and hence we use a conservative estimate of 176±40 ka as representative for the eruption.

4.2. Tephra composition and origin

All studied tephra samples are dominated by pumice particles and/or glass shards (Fig. 4). To characterize tephra glasses, we have obtained ~500 EPMA and 80 LA-ICP-MS analyses for both proximal and distal tephra deposits (Tables S1, S13-S17). In major element bi-plots, glasses from all six distal tephras form a single trend in the high-K rhyolitic field similar to that of glasses from the proximal Elbrus pumice and with higher K_2O contents compared to Keli Highland pumices (Fig. 5). Both distal and proximal glass compositions extend and partly overlap with the trend formed by the Elbrus bulk rock compositions, which have distinctively high-K compositions in comparison with the medium-K Kazbek rocks (Fig. 5). All analyzed glasses compositions dramatically differ from the ~40 ka Campanian Ignimbrite ash (CI/Y5) found in the LPS of Kostenki area to the north of our study sites, excluding their correlation (Fig. 5; Pyle et al., 2006).

A set of bi-plots comparing available major and trace element glass composition of proximal Elbrus and distal tephras is presented on Figs. 6 – 8. The glasses form coherent trends of increasing K_2O and decreasing FeO, MgO, Al_2O_3, TiO_2, Na_2O, and P_2O_5 at increasing SiO_2, typical for suites of peraluminous rhyolite glasses (e.g., Shiveluch volcano; Ponomareva et al., 2015), which are mostly controlled by crystallization of low-K_2O phases – plagioclase, pyroxenes, Fe-Ti oxides and apatite (±hornblende, ±quartz). The appearance of K-rich low-Ca phases (K-feldspar, biotite) on liquidus of Elbrus magmas is reflected in a slight change of the slope of glass trends at ~74 wt% SiO_2 (Fig. 6). The distal and proximal glasses overlap in the entire compositional range. It is, however, noticeable that the distal glasses mostly plot within the lower range of K_2O and TiO_2 in proximal glasses at given SiO_2 and in the upper range of Na_2O and Cl (Fig. 6). Post-magmatic low-temperature alteration of glass cannot explain these compositional variations because TiO_2 is an essentially immobile element during glass weathering (e.g., Jezek and Noble, 1978). It is more likely that our collection of distal Elbrus tephras is not fully representative for large explosive eruptions of Elbrus volcanic center, the presumed source for these distal tephras. The proximal counterparts of some distal tephras might be not preserved or not sampled so far.

Variations of selected trace elements (Rb, Sr, Zr, Ba) plotted versus SiO_2 in tephra glasses and in <1 Ma Elbrus lavas (Lebedev et al., 2010b; Chernyshev et al., 2014; Bindeman et al., 2021) are shown in Fig. 7. Similar to major elements, the proximal Elbrus and distal tephra glasses have overlapping compositions and form coherent trends with bulk rock (mostly lava) compositions. The trace element contents change systematically with SiO_2, and the trends are controlled by crystallization of major mineral phases present in the Elbrus rocks. Concentrations of Rb increase over the entire range of SiO_2 and illustrate the generally incompatible behavior of this element during magma crystallization dominated by low-K phases (Fig. 7a). Concentrations of Sr decrease steadily with increasing SiO_2 (Fig. 8b) consistent with the ubiquitous presence of Sr-rich plagioclase phenocrysts in Elbrus rocks (e.g., Lebedev et al., 2010a). Concentrations of Zr and Ba in the whole rocks remain within a relatively narrow range (Zr) or increase (Ba) with increasing SiO_2 (Fig. 8c, d). The negatively sloped trends defined by the tephra glasses indicate the appearance of zircon and K-feldspar on the liquidus of the most silicic Elbrus magmas (SiO_2>72 wt%) including rhyolite ignimbrites (e.g., Chernyshev et al., 2014; Bindeman et al., 2021).

The Elbrus affinity of the distal tephras is also illustrated by spidergrams of the average glass compositions (Fig. 8). The compositions normalized to primitive mantle coincide very closely with those of proximal tephras except some elements (Zr, Hf, Ti) in the most Si-rich distal glasses. Characteristic features of all Elbrus tephra glasses are moderately depleted and very slightly negatively sloped normalized spectra of heavy rare earth elements (from Dy to Lu), a relatively steeply sloped spectra of the light rare earth elements ($(La/Sm)_N$ = 4.9 – 6.8 for average compositions), pronounced minima of Sr, Ba, Nb, Ti, and strong enrichment in Th, U, Pb and Li. In comparison with typical Elbrus dacites, the glasses are significantly enriched in the most incompatible elements (Cs, Rb, Th, U, Pb), depleted in Sr, Eu, Ti, and contain similar amounts of other trace elements shown in Fig. 8. The difference between glass and whole rock compositions is consistent with the presence of relatively abundant plagioclase, pyroxene and Fe-Ti oxides in the Elbrus rocks.

The Sr-Nd-Pb isotope compositions of the studied distal tephras are shown in Fig. 9. The compositions are compared with literature data on lavas and ignimbrites from Elbrus and Kazbek volcanic centers and proximal pumice (Elbrus-5-5) analyzed in this study. The relatively high $^{87}Sr/^{86}Sr$, $^{207}Pb/^{204}Pb$, $^{208}Pb/^{204}Pb$ and low $^{143}Nd/^{144}Nd$ isotope ratios testify an Elbrus-type source for all studied tephras, which is strongly different from the Kazbek-type source (Fig. 9). In terms of Pb isotope compositions, the distal tephras show very close similarity with the Elbrus rocks and tephras.

4.3. Identified tephras

Four tephra deposits – one proximal pumice (Elbrus-5-5) and three distal ones (SARM, TMG, and OTK), revealed distinctly different eruption ages of 522±36, 258±13, 176±40, and 84.6±7.4 ka. Their geochemical compositions thus provide the reference values for the identification of undated distal tephras BU and VL.

Despite similar compositions, glasses from six distal tephras exhibit individual features that to some extent allow deciphering chemical characteristics by location. Glasses from SARM and TSK tephras form prominent trends in SiO_2 contents (from 69.5–71.5 to 77.3–78.3 wt%), while glasses from TMG, VL, and OTK tephras form clusters in the high-Si range (at SiO_2>75 wt% with a few lower-Si shards in VL) (Fig. 6). On the contrary, glasses from the BU tephra form a tight cluster in the low-Si field at SiO_2=71–73 wt% at slightly elevated K_2O compared to other distal glasses in the same SiO_2 range (Fig. 10a). TMG, VL, and OTK are similar in most elements with SiO_2 contents mostly in the range between 74.5 and 78 wt %.

However, OTK glasses have slightly higher K_2O and lower TiO_2 and Cl contents compared to other tephras (Fig. 6d, h).

In terms of Sr and Nd isotope compositions, TMG tephra is close to Elbrus lavas and proximal tephra with the highest $^{87}Sr/^{86}Sr$ and lowest $^{143}Nd/^{144}Nd$ (Fig. 9a). SARM tephra is similar to young (<1 Ma) Elbrus ignimbrites, whereas OTK and VL tephras have even more radiogenic Sr and less radiogenic Nd isotope compositions similar to Pliocene ignimbrites from the Elbrus area (Chernyshev et al., 2014). VL is a very fine-grained tephra with typical grain size of 50–100 µm (Fig. 4f). Thus, it cannot be excluded that the very radiogenic Sr isotope compositions of this tephra results from contamination by marine sediments, presumably composed by continentally derived material with $^{87}Sr/^{86}Sr$ ≈0.71–0.72 (Goldstein and Jacobsen, 1983). In contrast, OTK tephra is coarse sand, and contamination by loess hosting this tephra is very improbable. No young Elbrus samples reported thus far have, however, similarly enriched Sr and Nd isotope composition as the OTK tephra Fig. 9a). It should then be a very distinctive feature of this eruption.

The BU tephra is distinctly different from other distal tephras and plots in a lower-Si field compared to the other distal glasses but similar to most of glasses from the proximal site Elbrus-5 and a part of those from redeposited pumice Elbrus-6-1 (Fig. 10). The BU multi-element patterns fall into the field formed by Elbrus proximal tephra (Fig. 7). Thus, the stratified pumices from site Elbrus-5 (including the dated sample Elbrus-5-5) may represent a proximal counterpart for the BU distal tephra. In this case, the age of the BU tephra may be preliminary estimated at 176±40 ka. However, the chronological estimate needs further refinement (see section 4.1). Glasses from site Elbrus-6 are compositionally mixed and combine BU/Elbrus-5 low-Si glasses and high-Si glasses likely from different tephras (Fig. 10). This feature further confirms the redeposited nature of the Elbrus-6 deposits as already suggested by the field observations (Section 3.2; Supplementary Text).

The TSK tephra largely overlaps in its major element composition with the SARM tephra, but its field is shifted to lower SiO_2 contents than that of the SARM (Fig 6). The TSK tephra can be distinguished based on trace element data (e.g., higher B, lower V). The TSK should thus represent a different, so far undated, eruption.

The SARM tephra shows a wide range in SiO_2 composition, which is also observed for the VL tephra. At high silica contents (77–78 wt% SiO_2) both tephras overlap in their composition (Fig. 6). However, trace elements and isotope compositions do not fully confirm such correlation and rather suggest that these tephras contain compositionally different material. First, there is a pronounced difference in isotope composition of VL and SARM tephras (Fig. 9). As already mentioned, $^{87}Sr/^{86}Sr$ of VL tephra could be hypothetically explained by contamination of the bulk tephra sample by the host sediment (terrestrial/continental component in marine sediments). However, this process can hardly explain the slightly less radiogenic Pb isotope composition of VL tephra in comparison to the SARM tephra because average upper continental crust has relatively high Pb isotope ratios ($^{206}Pb/^{204}Pb \approx 19.3$, $^{207}Pb/^{204}Pb \approx 15.7$, $^{208}Pb/^{204}Pb \approx 39.3$) (Asmeron and Jacobsen, 1993), and thus contaminated samples should exhibit coherently elevated $^{87}Sr/^{86}Sr$ and, for example, $^{207}Pb/^{204}Pb$ isotope ratios. It seems more likely that the difference in the isotope compositions reflects different magma sources and/or different eruptions for the prevailing fraction of at least VL and SARM tephras. Nevertheless, despite the difference in bulk isotope composition, SARM and VL tephras contain glass shards, which have indistinguishable compositions and thus could readily originate from the same eruption (Figs. 11 and 12). In addition, both deposits are located northeast of the source, which suggests a similar ashfall axis, and have close previous age estimates (Table 1; Lavrushin et al., 1998; Sorokin et al., 2018). At this stage, we suggest that SARM and VL tephras may be provisionally correlated, however, a more detailed investigation is needed.

Thus, in the light of our results, we were able to identify four Elbrus tephras (OTK, TMG, BU, and SARM-VL) and single out one more Elbrus tephra of unknown age (TSK) (Table 1). From these tephras, BU, SARM-VL, and TSK have distinct geochemical characteristics, which permit their identification (Figs. 6 and 10). Tephras OTK and TMG are very similar and can be used as markers only under good chronostratigraphic control.

4. 4. Volcanological implications

Our geochemical and geochronological data permit the identification of the Elbrus volcanic center as the source of at least five different distal tephra deposits with tephra dispersal over more than 150–560 km from the source. This result points to a previously unrecognized period of powerful explosive eruptions from the Elbrus center with at least four large eruptions between ~522 and 85 ka. Four tephras (TMG, OTK, BU, and TSK) have been identified each in a single distal site whereas two tephras found ~340 km apart and 500–550 km from Elbrus (SARM and VL) may represent the same tephra (Fig. 1b; Table 1). Tephras TMG, OTK, BU, and TSK exhibit clear signs of redeposition into the gullies or depressions so we tried to estimate the initial tephra thickness where possible (Table 1; section 3.3). Based on these limited data we present the most conservative tephra volume estimates to evaluate the eruption magnitudes.

Minimum estimates of tephra volumes based on the single-isopach method by Legros (2000) are 2.2 km^3 for TMG, 4.5 km^3 for OTK, 5.1 km^3 for BU, and as much as 404 km^3 for SARM-VL. Corresponding eruption magnitudes (M) calculated according to Pyle et al. (1995) are: TMG=5.2, OTK=5.7, BU=5.6, and SARM-VL=7.5. Volume of TSK tephra is hard to estimate as the original thickness of this thinly laminated ash (Fig. 2f, g) is unknown. New findings of those tephras may increase the area of ash-fall and change volume estimates dramatically.

The extraordinary large volume estimate for the SARM-VL tephra is based on the tentative geochemical correlation of these deposits and their measured thicknesses (0.75 m and 0.7 m, respectively). Even if the correlation was invalid (see section 4.3), the volumes and magnitudes calculated by the same method for SARM and VL separately (111 and 147 km^3, and M 6.98 and M 7.0, respectively) would be far larger than for other Elbrus tephras. Both tephras were deposited into the sea and in spite of their great thicknesses do not exhibit signs of redeposition (Lavrushin et al., 1998; this study). Further research including identification of these tephras in the terrestrial deposits is required to validate these thickness values and corresponding tephra volumes. However, our calculations show that even a tenfold increase of primary ash-fall thickness would increase an estimate of eruption magnitude by only one unit. In other words, SARM and VL eruptions, even if taken separately, still significantly exceed in magnitude any other known Elbrus eruption. The eruption of such scale, comparable with the M 7.0 Tambora one, might have caused hemisphere-scale climatic impact recorded by paleogeographic proxies across Eurasia.

Existence of middle to late Pleistocene large-scale explosive volcanism in the Elbrus area is not surprising as earlier large explosive eruptions occurred in this area repetitively and deposited Chegem ignimbrite and two ignimbrite units in the Elbrus area (Lipman et al., 1995; Chernyshev et al., 2014). However, no distal tephras associated with these eruptions were documented, and thus their erupted volumes and tephra dispersal remain unknown.

Our age estimates for four large explosive eruptions (522±36, 258±13, 176±40, and 84.6±7.4 ka) suggest that two older eruptions occurred beyond the active periods suggested so far for the Elbrus volcanic center based on lava and welded tuff dating (950–900, 840–700, 225–170, 110–70 ka, and <30 ka; Lebedev et al., 2010a; Chernyshev et al., 2014) (Fig. 13). Two younger eruptions took place in the second half of respective active periods. These results highlight the importance of tephra studies for a more comprehensive understanding of the eruptive histories of potentially active volcanoes.

4. 5. Tephrochronological implications for paleoenvironmental archives

The geochemically characterized and dated tephra deposits from our study were found in different paleoenvironmental settings including loess sequences (TMG and OTK), marine (SARM and VL), and paleolake (TSK) sediments, and on the top of the fluvial deposits (BU) (Table S1, Supplementary Text). Below we present the first insights into the merit of these tephras as markers for European paleoenvironmental research.

Tephra in loess-paleosol successions. Loess-paleosol sequences (LPS) are among the main terrestrial archives of the paleoenvironmental change during the Pleistocene (Velichko, 1990; Muhs, 2013; Marković et al., 2015; Pye et al., 1995). However, these spatially extensive depositional successions often contain erosional gaps and are quite difficult to date (e.g., Marković et al. 2018; Konstantinov et al., 2018; Stevens et al., 2018). Loess sediments are widely spread on the plains north of the Greater Caucasus Range, reaching a thickness of 100–140 m, which places them among the thickest LPS in Europe (Astakhov et al., 2022; Trofimov et al., 2008). Long-term studies of these deposits, mainly in the western part of the area, near Azov Sea, permitted the elaboration of a summary stratigraphy where the major loess horizons correspond to glaciations and most of the paleosol layers to interglacials (Velichko et al., 2009, 2012, 2017). This stratigraphy is being continuously refined based on paleopedological, paleontological, paleomagnetic, and other data as well as radiocarbon, luminescence, and amino acid geochronology (e.g., Liang et al., 2016; Panin et al., 2018; Tesakov et al., 2020; Mazneva et al., 2021). However, very few direct dates older than the last 130 ka are available (e.g., Chen et al., 2018a, b).

As numerous European examples suggest, targeted tephra and cryptotephra research in the LPS could significantly facilitate the correlation of disparate outcrops (e.g., Bösken et al., 2017; Marković et al., 2018; Lomax et al., 2019). One of the best tephra links for European LPS is the CI/Y5 tephra related to the ~40 ka Campanian Ignimbrite eruption (e.g., Veres et al., 2013; Timar-Gabor et al., 2017; Pötter et al., 2021). However, in the East European Plain its potential is still underutilized as it was geochemically fingerprinted only in the Kostenki area (Pyle et al., 2006). Our new data on Elbrus tephras may contribute to the tephrochronological model for the European LPS.

OTK tephra: Middle Pleistocene OTK tephra (522±36 ka) was found close to the bottom of the Otkaznoe LPS (Figs. 2b, c) that is described as unique in its stratigraphic completeness paleoenvironmental archive (Trofimov et al., 2008; Bolikhovskaya, 1995, Bolikhovskaya et al., 2016; Sychev et al., 2022). The obtained age for the OTK tephra places it close to the marine isotope stage (MIS) 14/13 boundary. Earlier investigators of the same outcrop described ash pods ~0.7 km to the north-east of our site in the basal part of paleosol complex VI attributed to the MIS 17/16 boundary (Bolikhovskaya, 1995; Bolikhovskaya et al., 2016), which corresponds to ~676 ka (Lisiecki and Raymo, 2005). If these ash pods also represent our OTK tephra, our new date may require reconsideration of the published loess-paleosol chronostratigraphy for this key site making the paleosol complex VI and adjacent loess units ~150 ka younger. Further research on tephra lenses and pods in the bluffs and sedimentary cores in this area will help in deciphering the complexities of the LPS stratigraphy.

TMG tephra: Middle Pleistocene TMG tephra (258±13 ka) lies inside the filling of an ancient gully within the LPS (Fig. 2d, e). As this tephra lens is composed mostly of clean ash, the redeposition likely took place almost simultaneously with the tephra fall. The tephra is overlain by LPS, which includes two weakly expressed and one well developed paleosols. The well expressed paleosol yielded a radiocarbon date of 17400±1000 a BP, which allowed

Melekestsev et al. (2005) to suggest an age for TMG tephra of ~22 cal ka (calibrated value). However, the normal LPS stratigraphy in the area suggests that the well-developed paleosol formed no later than MIS 5c (Velichko et al., 2009, 2012, 2017; Panin et al., 2018; Mazneva et al., 2021). This implies a far older age of the TMG tephra than the earlier suggested 22 ka.

Our date of 258±13 ka suggests that the TMG tephra was deposited within MIS 8, close to the MIS 8/7 boundary. As the existing stratigraphic schemes for this period offer at least three competing variants of the MIS assignment for the LPS units within the Saalian stage (Velichko and Morozova, 2010; Bolikhovskaya et al., 2016; Zastrozhnov et al., 2017), further search for the TMG tephra and cryptotephra in the reference outcrops might help to resolve this discrepancy. In addition, TMG tephra suggests and dates a previously unknown incision of the ancient fluvial network (Panin et al., 2020).

<u>The tephra SARM-VL in the Caspian Sea deposits.</u> The modern Caspian Sea is the world's largest inland body of water, a relic of the ancient Paratethys Sea, lying ~27 m below sea level. In the past, the sea went through a series of rapid transgressions and regressions, with Pleistocene water levels changing from -150 to +80 m a.s.l. (Krijgsman et al., 2019). Studies of the marine sediments recovered by drill cores in the northern part of the Caspian Sea have allowed reconstructions of the sea evolution with major transgressions-regressions dated mostly by biostratigraphy and supplemented by some radiocarbon dates for the youngest (<55 ka) deposits (Bezrodnykh et al., 2015; Sorokin et al., 2018; Yanina et al., 2018, 2021). No visible tephras from the Caspian sediments have ever been reported although they were found in many adjacent on-shore regions (e.g., Karlov, 1957; Ganzei, 1987; Lavrushin et al., 1998). Our first marine finding, the late Pleistocene SARM tephra (84.6±7.4 ka) deposit (Fig. 1b) immediately underlies the sediments of the Hyrcanian (Girkanian) transgression – the least studied and most controversial period of the Caspian Sea history with a provisional age estimate of ~80 ka (Popov, 1955, 1967; Goretskiy, 1957; Yanina, 2013; Sorokin et al., 2018).

This transgression is characterized by a specific brackish-water mollusk assemblage, with some freshwater species, high sea stand of +9 m, and northward sea advance for 250 km (Yanina et al., 2014; Sorokin et al., 2018; Krijgsman et al., 2019). The Hyrcanian mollusk fauna shows that during this transgression Caspian waters drained to the Black Sea through the Manych Strait (Fig. 1b; Popov, 1983; Yanina, 2014). The attempts to date the Hyrcanian deposits by radiocarbon returned an age estimate of >55 ka, which means that the transgression lies beyond the capacity of the method. The lack of direct age data hampered placing accurate temporal constraints on the transgression age and its correlation with certain MIS.

Our newly obtained age of 84.6±7.4 ka for the SARM tephra is the first direct age determination for the lower boundary of the Hyrcanian deposits and for the rapid onset of the transgression suggesting that it started as early as MIS 5c-a. Proposed correlations of this deposit to the VL tephra, lying within the paleo-delta slope deposits ~250 km upstream the Volga River, permits the insight into the extent of the Hyrcanian transgression and correlations between deep sea and delta deposits.

5. Conclusions

Geochemical studies and zircon double dating (ZDD) of the pumiceous tephra deposits sampled along the southeast European margin have allowed us to identify five individual tephras with slightly different glass compositions and link them to the Elbrus volcanic center (Greater Caucasus) based on their geochemical similarity to its proximal deposits. Four of these eruptions were dated at 522±36, 258±13, 176±40, and 84.6±7.4 ka, which suggests the repetitive accumulation of large magma volumes beneath the volcano and subsequent powerful explosive eruptions well after the formation of the earlier known ~800 ka old silicic ignimbrites. Tephras of these eruptions were dispersed over more than 150–560 km from the source, which suggests conservative eruption magnitudes of 5.2–7.5. The largest eruption was probably associated with the deposition of the 84.6±7.4 ka old SARM-VL tephra. An eruption of such scale might have caused hemisphere-scale climatic impact and have been recorded by paleogeographic proxies across Eurasia.

Each of the identified tephras has its paleogeographical value and can be used to decipher the complexities of both terrestrial and marine stratigraphy. The OTK and TMG tephras date close to the MIS 14/13 and MIS 8/7 boundaries, respectively. However, as compositions of these tephras are quite similar, their use as markers must be supported by stratigraphic constraints. The BU tephra is compositionally unique; however, its age estimate, although it firmly places it between the TMG and SARM tephras, is quite loose and needs refinement. The SARM tephra (probably correlating to VL) is a marker for the rapid onset of the Hyrcanian transgression of the Caspian Sea. Stratigraphic position and the age of as yet undated TSK tephra needs further examination.

Our data provide the first geochemical characterization of both proximal and distal Elbrus tephra glasses and contribute to the global tephra database, permitting the identification of Elbrus tephras in distal terrestrial and marine paleoenvironmental archives and their use as markers in paleoclimate and archaeological research.

Acknowledgements

MP, FH, SM, and DGS were supported by the German Research Foundation grant #GA1960/14-1. VP, EZ, and EK acknowledge support from the Russian Foundation for Basic Research grant #20-55-12011, which permitted collection of tephra samples as well as data analysis and writing of the manuscript. The study was also supported in part by the Megagrant project (agreement № 075-15-2021-599, 8.06.2021) and the Institute of Geography AAAA-A19-119021990092-1 (FMWS-2019-0008) program, which covered the paleogeographic studies. Laboratory assistance of Mario Thöner and Ulrike Westernströer with EPMA and LA-

ICP-MS analyses and Silke Hauff with TIMS is kindly acknowledged. The authors thank Viktor Gazeev and Vasily Lavrushin for sharing their tephra samples and Andrei Zakharov, Nikita Sychev, and Elena Mazneva for their help with the fieldwork. The authors appreciate the constructive reviews by B. Giaccio and by an anonymous reviewer.

References

Albert P.G., Giaccio B., Isaia R., Costa A., Niespolo E.M., Nomade S., Pereira A., Renne P.R., Hinchliffe A., Mark D.F., Brown R.J., 2019. Evidence for a large-magnitude eruption from Campi Flegrei caldera (Italy) at 29 ka. Geology. 47(7): 595-9.

Asmerom Y., Jacobsen S.B., 1993. The Pb isotopic evolution of the Earth: inferences from river water suspended loads. Earth Planet. Sci. Lett., 115(1): 245-256 https://doi.org/10.1016/0012-821X(93)90225-X

Astakhov, V., Pestova, L., Shkatova, V., 2022. Loessoids of Russia: Varieties and distribution. Quat. Int., 620: 24-35. https://doi.org/10.1016/j.quaint.2021.01.005

Bewick S., Parkinson I.J., Harris N., Adamia S., Sadradze N., Allen M.B., Hammond S., 2022. Quaternary collision-zone magmatism of the Greater Caucasus. Journal of Petrology, 63(5), p.egac037. https://doi.org/10.1093/petrology/egac037

Bezrodnykh Yu.P., Deliya S.V., Romanyuk B.F., Sorokin V.M., Yanina T.A., 2015. New Data on the Upper Quaternary Stratigraphy of the North Caspian Sea. Doklady Earth Sciences, 462, 1, 479-483.

Bindeman I.N., Colón, D.P., Wotzlaw, J.F., Stern, R., Chiaradia, M. and Guillong, M., 2021. Young Silicic Magmatism of the Greater Caucasus, Russia, with implication for its delamination origin based on zircon petrochronology and thermomechanical modeling. J. Volcanol. Geotherm. Res., 412: 107173.

Bogatikov O.A., Gurbanov A.G., Katov D.M., Melekestsev I.V., Puriga A.I., 1998. The Elbrus caldera in the northern Caucasus. Dokl. Earth Sci. 363, 1202–1204.

Bogatikov O.A., Melekestsev I.V., Gurbanov, A.G., Sulerzhitsky L.D., Koshchug D.G., Grün R.V., Chernych V.I., Arakeliantz M.M., Kirianov V.Yu., Gazeev V.M., Gurbanov A.A., Puriga A.I., Trusov A.V., 2001. Catastrophic Pleistocene and Holocene activity of the Elbrus volcanic center (Northern Caucasus, Russia): events and chronology based on the 14C, ESR, and K-Ar dating. Volcanology and Seismology, 2: 3-17 [In Russian]

Bolikhovskaya N.S., 1995. Evolution of the loess-soil formation of the Northern Eurasia. Moscow, Moscow University Publishers, 270 p. [In Russian]

Bolikhovskaya N.S., Faustov S.S., Markova A.K., 2016. Pleistocene climatic stratigraphy and environments of the Terek-Kuma Lowland (NW Caspian sea region) inferred from palynological, paleomagnetic and rodent records of the long Otkaznoye sediment sequence. Quat. Int. 409: 16-32. https://doi.org/10.1016/j.quaint.2015.09.067

Bösken J., Klasen N., Zeeden C., Obreht I., Marković S.B., Hambach U., Lehmkuhl F., 2017. New luminescence-based geochronology framing the last two glacial cycles at the southern limit of European Pleistocene loess in Stalać (Serbia). Geochronometria, 44(1): 150-161.

Chen J., Yang T., Matishov G.G., Velichko A.A., Zeng B., He Y., Shi P., Fan Z., Titov V.V., Borisova O.K., Timireva S.N., 2018a. A luminescence dating study of loess deposits from the Beglitsa section in the Sea of Azov, Russia. Quat. Int., 478, pp.27-37. https://doi.org/10.1016/j.quaint.2017.11.017

Chen J., Yang T.B., Matishov G.G., Velichko A.A., Zeng B., He Y., Shi P.H., 2018b. Luminescence chronology and age model application for the upper part of the Chumbur-Kosa loess sequence in the Sea of Azov, Russia. Journal of Mountain Science, 15(3): 504-518. https://doi.org/10.1007/s11629-017-4689-0

Chernyshev, I.V., Bubnov, S.N., Lebedev, V.A., Gol’tsman, Yu.V., Bairova, E.D., Yakushev, A.I., 2014. Two stages of explosive volcanism of the Elbrus area: Geochronology, petrochemical and isotopic-geochemical characteristics of volcanic rocks, and their role in the Neogene-Quaternary evolution of the Greater Caucasus. Stratigr. Geol. Correl. 22, 96–121. https://doi.org/10.1134/S086959381401002X

Chugaev A.V., Chernyshev I.V., Lebedev V.A., Eremina A.V. (2013) Lead Isotope composition and origin of the quaternary lavas of Elbrus Volcano, the Greater Caucasus: High-precision MC-ICP-MS data. Petrology 21(1):16-27 doi:10.1134/S0869591113010037

Cullen V.L., Smith V.C., Tushabramishvili N., Mallol C., Dee M., Wilkinson K.N., Adler D.S., 2021. A revised AMS and tephra chronology for the Late Middle to Early Upper Paleolithic occupations of Ortvale Klde, Republic of Georgia. Journal of Human Evolution, 151: 102908. https://doi.org/10.1016/j.jhevol.2020.102908

Danišík M., Schmitt A.K., Stockli D.F., Lovera O.M., Dunkl I., Evans N.J., 2017. Application of combined U-Th-disequilibrium/U-Pb and (U-Th)/He zircon dating to tephrochronology. Quat. Geochronol., 40, pp.23-32. https://doi.org/10.1016/j.quageo.2016.07.005

Danišík M., Lowe D.J., Schmitt A.K., Friedrichs B., Hogg A.G., Evans N.J., 2020. Sub-millennial eruptive recurrence in the silicic Mangaone Subgroup tephra sequence, New Zealand, from Bayesian modelling of zircon double-dating and radiocarbon ages. Quat. Sci. Rev., 246: 106517.

Deligne N., Coles S., Sparks R., 2010. Recurrence rates of large explosive volcanic eruptions. J. Geophys. Res.: Solid Earth (1978–2012) 115. https://doi.org/10.1029/2009JB006554

Doronicheva, E.V., Golovanova, L.V., Doronichev, V.B., Nedomolkin, A.G., Korzinova, A.S., Tselmovitch, V.A., Kulkova, M.A., Odinokova, E.V., Shirobokov, I.G., Ivanov, V.V. and

Nesmeyanov, S.A., 2019. The first laminar Mousterian obsidian industry in the north-central Caucasus, Russia (preliminary results of a multi-disciplinary research at Saradj-Chuko Grotto). Archaeological Research in Asia, 18: 82-99. https://doi.org/10.1016/j.ara.2019.03.001

Goretskiy G.I., 1957. About Hyrcanian epoch in the history of Pre-Caspian region. News Oil Eng. 6, 6–11 [In Russian].

Ganzei S.S. 1987. Late Cenozoic deposits of the Ponto-Caspian region and the fission-track dating of volcanic ashes. In: Fisson-track Method in Geology and Geography. Vladivostok, Far East Scientific Center of the USSR. P. 33-45 [in Russian].

Gazeev V.M. and Gurbanov A.G., 2004. Geological Map of the Elbrus volcanic structure. In: Laverov, N.P. (Ed.), Natural Processes on the Territory of Kabardino-Balkaria. Moscow IGEM RAN 438p. [in Russian].

Gazeev V.M., Gurbanov A.G., Leksin A.B., Dokuchaev A.Ya., Isakov S.I., 2011. Pliocene-Quaternary ashes at the territory of the Southern Federal District (problems, paradoxes, ideas). Vestnik of the Vladikavkaz Science Center, II(3): 39-47 [In Russian]

Gazis C.A., Lanphere M., Taylor H.P., Gurbanov A., 1995. 40Ar/39Ar and 18O/16O studies of the Chegem ash-flow caldera and the Eldjurta Granite: Cooling of two late Pliocene igneous bodies in the Greater Caucasus Mountains, Russia. Earth Planet. Sci. Lett. 134, 377–391.

Giaccio, B., Leicher, N., Mannella, G., Monaco, L., Regattieri, E., Wagner, B., Zanchetta, G., Gaeta, M., Marra, F., Nomade, S., Palladino, D. M., Pereira, A., Scheidt, S., Sottili, G., Wonik, T., Wulf, S., Zeeden, C., Ariztegui, D., Cavinato, G. P., Dean, J. R., Florindo, F., Leng, M. J., Macri, P., Niespolo, E., Renne, P. R., Rolf, C., Sadori, L., Thomas, C. & Tzedakis, P. C. 2019: Extending the tephra and palaeoenvironmental record of the Central

Mediterranean back to 430 ka: A new core from Fucino Basin, central Italy. Quaternary Science Reviews 225, 106003.

Goldstein SJ, Jacobsen SB (1988) Nd and Sr isotopic systematics of river water suspended material: implications for crustal evolution. Earth Planet. Sci. Lett. 87(3):.249-265

Golovanova L.V., Doronichev V.B., Cleghorn N.E., Koulkova M.A., Sapelko T.V., Shackley M.S., 2010. Significance of ecological factors in the Middle to Upper Paleolithic transition. Current Anthropology, 51(5): 655-691.

Gurbanov A.G., Bogatikov O.A., Melekestsev I.V., Lipman P.W., Lowenstern J.B., Miller D.R., Dokuchaev A.Y., 2004. The Elbrus Caldera in the Northern Caucasus: Geological structure and time of formation. Russ. J. Earth Sci. 6: 251–255. https://doi.org/10.2205/2004ES000161

Haeberli W., Huggel C., Kääb A., Zgraggen-Oswald S., Polkvoj A., Galushkin I., Zotikov I., Osokin N., 2004. The Kolka-Karmadon rock/ice slide of 20 September 2002: an extraordinary event of historical dimensions in North Ossetia, Russian Caucasus. J. Glaciol., 50(171): 533-546. https://doi.org/10.3189/172756504781829710

Hidjrati N.I., Kimball L.R., Koetje T., 2003. Middle and Late Pleistocene investigations of Myshtulagty Lagat (Weasel Cave) North Ossetia, Russia. Antiquity, 77(298): 1-5.

Jezek P. A. and Noble, D. C., 1978. Natural Hydration and Ion-Exchange of Obsidian - Electron-Microprobe Study. American Mineralogist 63: 266-273.

Kaigorodova E.N., Lebedev V.A., Chernyshev I.V., Yakushev A.I., 2021. Neogene–Quaternary magmatism in Eastern Balkaria (North Caucasus, Russia): evidence from the isotope–geochronological data. Doklady Earth Sciences, 496(1): 37-44.

Karátson, D., Wulf, S., Veres, D., Magyari, E.K., Gertisser, R., Timar-Gabor, A., Novothny, Á., Telbisz, T., Szalai, Z., Anechitei-Deacu, V. and Appelt, O., 2016. The latest explosive eruptions of Ciomadul (Csomád) volcano, East Carpathians—a tephrostratigraphic approach for the 51–29 ka BP time interval. J. Volcanol. Geotherm. Res., 319: 29-51. https://doi.org/10.1016/j.jvolgeores.2016.03.005

Karlov N.N., 1957. On the history of the study of the volcanic ashes of the European part of the USSR. Bulletin of the Moscow Nature Research Society (Onshchestvo Ispytatelei Prirody), Geology Section, XXXII(2): 25-47 [In Russian].

Költringer C, Stevens T, Bradák B, Almqvist B, Kurbanov R, Snowball I, Yarovaya S., 2021. Enviromagnetic study of Late Quaternary environmental evolution in Lower Volga loess sequences, Russia. Quat. Res., 103: 49-73.

Konstantinov E.A., Velichko A.A., Kurbanov R.N., Zakharov A.L., 2018. Middle to Late Pleistocene topography evolution of the North-Eastern Azov region. Quat. Int., 465: 72-84. https://doi.org/10.1016/j.quaint.2016.04.014

Kraevaya T.S., 1985. Genetic types of the Pleistocene and Holocene Elbrus deposits. Volcanology and Seismology, 6: 20-32 [In Russian]

Krijgsman W., Tesakov A., Yanina T., Lazarev S., Danukalova G., Van Baak C.G.C, Agustí J., Alçiçek M.C., Aliyeva E., Bista D., Bruch A., Büyükmeriç Y., Bukhsianidze M., Flecker R., Frolov P., Hoyle T.M., Jorissen E.L., Kirscher U., Koriche S.A., Kroonenberg S.B., Lordkipanidze D., Oms O., Rausch L., Singarayer J., Stoica M., van de Velde S., Titov V.V., Wesselingh F.P., 2019. Quaternary time scales for the Pontocaspian domain: interbasinal connectivity and faunal evolution. Earth-Science Reviews, 188: 1-40. https://doi.org/10.1016/j.earscirev.2018.10.013

Lavrushin V.Yu., Lavrushin Yu.A., Antipov M.P., 1998. First finding of the volcanic ash in the Quaternary deposits of the lower Volga. Lithology and Mineral Deposits (Litologiya I Poleznye Iskopaemye), 2: 207-218 [In Russian]

Lazarev S., Kuiper K.F., Oms O., Bukhsianidze M., Vasilyan D., Jorissen E.L., Bouwmeester M.J., Aghayeva V., Van Amerongen A.J., Agustí J., Lordkipanidze, D., 2021. Five-fold expansion of the Caspian Sea in the late Pliocene: New and revised magnetostratigraphic and 40Ar/39Ar age constraints on the Akchagylian Stage. Global Planetary Change, 206, p.103624.

Lebedev V.A., Chernyshev I.V., Bubnov S.N., Medvedeva E.S., 2006. Chronology of magmatic activity of the Elbrus volcano (Greater Caucasus): evidence from K-Ar Isotope dating of lavas. Doklady Earth Sciences, Vol. 405(9): 1321.

Lebedev V.A., Chernyshev I.V., Chugaev A.V., Gol’tsman Y.V., Bairova E.D., 2010a. Geochronology of eruptions and parental magma sources of Elbrus volcano, the Greater Caucasus: K-Ar and Sr-Nd-Pb isotope data. Geochemistry International, 48(1): 41-67. https://doi.org/10.1134/S0016702910010039

Lebedev V.A., Sakhno V.G., Yakushev A.I., 2010b. Total duration and spatial migration of Quaternary volcanism in the El'brus region, Greater Caucasus. Doklady Earth Sciences, Vol. 430(1): 80. https://doi.org/10.1134/S1028334X10010186

Lebedev V.A., Bubnov S.N., Yakushev A.I., 2011a. Magmatic activity within the Northern Caucasus in the Early Neopleistocene: active volcanoes of the Elbrus center, chronology, and character of eruptions. Doklady Earth Sciences, Vol. 436(1): 32.

Lebedev V.A., Vashakidze G.T., Arutyunyan E.V., Yakushev A.I., 2011b. Geochronology and evolution of Quaternary volcanism at the Keli Highland, Greater Caucasus. Geochemistry International, 49(11):1120-1144. https://doi.org/10.1134/S0016702911090035

Lebedev V.A. and Vashakidze G.T., 2014. The catalogue of Quaternary volcanoes of the Greater Caucasus based on geochronological, volcanological and isotope-geochemical data. Journal of Volcanology and Seismology, 8(2): 93-107. https://doi.org/10.1134/S0742046314020043

Lebedev V.A., Dudauri O.Z., Gol’tsman Y.V., 2017. Early Pleistocene magmatism in the central part of the Greater Caucasus. Doklady Earth Sciences, Vol. 477(1): 1265-1269. https://doi.org/10.1134/S1028334X17110149

Lebedev V.A., Parfenov A.V., Vashakidze G.T., Gabarashvili Q.A., Chernyshev I.V., Togonidze M.G., 2018. Chronology of magmatic activity and petrologic–mineralogical characteristics of lavas of Kazbek Quaternary Volcano, Greater Caucasus. Petrology, 26(1): 1-28. https://doi.org/10.1134/S086959111801006X

Legros F., 2000. Minimum volume of a tephra fallout deposit estimated from a single isopach. J. Volcanol. Geotherm. Res. 96: 25-32. https://doi.org/10.1016/S0377-0273(99)00135-3.

Leicher, N., Giaccio, B., Zanchetta, G., Sulpizio, R., Albert, P. G., Tomlinson, E. L., Lagos, M., Francke, A. & Wagner, B. 2021: Lake Ohrid's tephrochronological dataset reveals 1.36 Ma of Mediterranean explosive volcanic activity. Scientific Data 8, 231.

Le Maitre R.W., Streckeisen A., Zanetti B., Le Bas M.J., Bonin B., Bateman P., Bellieni G., Dudek A., Efremova S., Kelle, J., Lameyre J., Sabine P.A., Schmid R., Soerensen H., Wooley A.R. (Eds.), 2002. Igneous Rocks. A Classification and Glossary of Terms. Cambridge University Press.

Liang Y., Yang T.B., Velichko A.A., Zeng B., Shi P.H., Wang L.D., He Y., Chen J., Chen Y., 2016. Paleoclimatic record from Chumbur-Kosa section in Sea of Azov region since marine isotope stage 11. J. Mountain Sci., 13(6): 985-999. https://doi.org/10.1007/s11629-015-3738-9

Lisiecki L.E. and Raymo M.E., 2005. A Pliocene-Pleistocene stack of 57 globally distributed benthic δ18O records. Paleoceanography, 20(1).

Lipman P.W., Bogatikov O.A., Tsvetkov A.A., Gazis C., Gurbanov A.G., Hon K., Koronovsky N.V., Kovalenko V.I., Marchev P., 1993. 2.8-Ma ash-flow caldera at Chegem River in the northern Caucasus Mountains (Russia), contemporaneous granites, and associated ore deposits. J. Volcanol. Geotherm. Res., 57(1-2): 85-124. https://doi.org/10.1016/0377-0273(93)90033-N

Lomax J., Fuchs M., Antoine P., Rousseau D.D., Lagroix F., Hatté C., Taylor S.N., Till J.L., Debret M., Moine O., Jordanova D., 2019. A luminescence-based chronology for the Harletz loess sequence, Bulgaria. Boreas, 48(1): 179-194.

Ludwig K.R. and Mundil R., 2002. Extracting reliable U-Pb ages and errors from complex populations of zircons from Phanerozoic tuffs. Geochim. Cosmochim. Acta, 66(15A): A463-A463.

Marković S.B., Stevens T., Kukla G.J., Hambach U., Fitzsimmons K.E., Gibbard P., Buggle B., Zech M., Guo Z., Hao Q., Wu H., 2015. Danube loess stratigraphy—Towards a pan-European loess stratigraphic model. Earth-Science Reviews, 148: 228-258.

Marković S.B., Stevens T., Mason J., Vandenberghe J., Yang S., Veres D., Újvári G., Timar-Gabor A., Zeeden C., Guo Z., Hao Q., 2018. Loess correlations – Between myth and reality. Palaeogeogr. Palaeoclimatol. Palaeoecol. 509: 4-23.

Matsapulin V.U., Yusupov A.R., Cherkashin V.I., 2008. Late Cenozoic volcanism of the Northern margin of the Eastern Caucasus orogeny (Dagestan). Vestnik of the Dagestan Science Center, 32: 12-20 [In Russian].

Mazneva E., Konstantinov E., Zakharov A., Sychev N., Tkach N., Kurbanov R., Sedaeva K., Murray, A., 2021. Middle and Late Pleistocene loess of the Western Ciscaucasia: Stratigraphy, lithology and composition. Quat. Int., 590: 146-163. https://doi.org/10.1016/j.quaint.2020.11.039

McDonough W.F., Sun S.S., 1995. The Composition of the Earth. Chem. Geol. 120(3-4): 223-253. https://doi.org/10.1016/0009-2541(94)00140-4

Melekestsev I.V., Kirianov V.Yu., Praslov N.D., 1988. Catastrophic eruption in the region of the Flegrei fields (Italy) as a possible source of the volcanic ash in the Upper Pleistocene deposits in the European part of the USSR. Volc Seis 6(3): 393-406.

Melekestsev I.V., Gurbanov A.G., Kirianov V.Yu., Chernych V.I., Sulerzhitsky L.D., Zaretskaya N.E., 2005. Volcanic ashes of the late Pleistocene catastrophic eruptions at the territory of the Eastern and Southern Europe. In: N.P. Laverov (Ed) Recent and modern volcanism at the territory of Russia. Nauka Publishers, Moscow, pp 45-62 [In Russian]

Muhs D.R., 2013. The geologic records of dust in the Quaternary. Aeolian Research, 9: 3-48. https://doi.org/10.1016/j.aeolia.2012.08.001

Panin P.G., Timireva S.N., Morozova T.D., Kononov Y.M., Velichko A.A., 2018. Morphology and micromorphology of the loess-paleosol sequences in the south of the East European plain (MIS 1–MIS 17). Catena, 168: 79-101. https://doi.org/10.1016/j.catena.2018.01.032

Panin A., Borisova O., Konstantinov E., Belyaev Y., Eremenko E., Zakharov A., Sidorchuk A., 2020. The Late Quaternary evolution of the upper reaches of fluvial systems in the southern East European Plain. Quaternary, 3(4): 31. https://doi.org/10.3390/quat3040031

Parfenov A.V., Lebedev V.A., Chernyshev I.V., Vashakidze G.T., Yakushev A.I., Goltsman Y.V., Chugaev A.V., Oleynikova T.I., Kanunnikova E.M., Gabarashvili Q.A. (2019) Petrological-geochemical characteristics of lavas, sources and evolution of magmatic melts of the Kazbek neovolcanic center (Greater Caucasus). Petrology, 27(6): 606-632. https://doi.org/10.31857/s0869-5903276658-689

Ponomareva V., Portnyagin M., Pevzner M., Blaauw M., Kyle Ph., Derkachev A. 2015. Tephra from andesitic Shiveluch volcano, Kamchatka, NW Pacific: Chronology of explosive eruptions and geochemical fingerprinting of volcanic glass. Int. J. Earth Sci. 104: 1459-1482. doi: 10.1007/s00531-015-1156-4.

Popov G.I., 1955. History of the Manych Strait in connection with a stratigraphy of the Black Sea and Caspian Sea deposits. Bull. MOIP. Dep. Geol. 20, 31-49 [In Russian].

Popov G.I., 1967. Hyrcanian transgression in the Northern Caspian Sea. Bull. Comm. Stud. Quat. Period 33, 77-86 [In Russian].

Popov G.I., 1983. The Pleistocene of the Black Sea - Caspian Sea Straits. Nauka Press, Moscow [In Russian].

Portnyagin M.V., Ponomareva V.V., Zelenin E.A., Bazanova L.I., Pevzner M.M., Plechova A.A., Rogozin A.N., and Garbe-Schönberg D., 2020. TephraKam: geochemical database of glass compositions in tephra and welded tuffs from the Kamchatka volcanic arc (northwestern Pacific). Earth System Science Data, 12(1): 469-486. https://doi.org/10.5194/essd-12-469-2020

Pötter S., Veres D., Baykal Y., Nett J.J., Schulte P., Hambach U., Lehmkuhl F., 2021. Disentangling sedimentary pathways for the Pleniglacial Lower Danube loess based on geochemical signatures. Frontiers in Earth Science, 9: 150.

Pye K., 1995. The nature, origin and accumulation of loess. Quat. Sci. Rev., 14(7-8): 653-667.

Pyle D.M., 1995. Assessment of the minimum volume of tephra fall deposits. J. Volcanol. Geotherm. Res. 69: 379-382. https://doi.org/10.1016/0377-0273(95)00038-0.

Pyle D.M., Ricketts G.D., Margari V., van Andel T.H., Sinitsyn A.A., Praslov N.D., Lisitsyn S., 2006. Wide dispersal and deposition of distal tephra during the Pleistocene 'Campanian Ignimbrite/Y5'eruption, Italy. Quat. Sci. Rev., 25(21-22): 2713-2728.

Rougier J., Sparks S.R., Cashman, K.V., 2016. Global recording rates for large eruptions. J. Applied Volcanol., 5(1): 1-10. https://doi.org/10.1186/s13617-016-0051-4

Rudnick R.L., Gao S., 2003. Composition of the Continental Crust. In: Treatise on Geochemistry vol 3. Elsevier Ltd., pp 1-64

Sambridge M.S. and Compston W., 1994. Mixture modeling of multi-component data sets with application to ion-probe zircon ages. Earth Planet. Sci Lett. 128(3-4), pp.373-390.

Self S., and Gertisser R., 2015. Tying down eruption risk. Nature Geosci. 8, 248-250. https://doi.org/10.1038/ngeo2403

Sherriff J.E., Wilkinson K.N., Harding P., Hawkins H., Timms R.G., Adler D.S., Beverly E.J., Blockley S.P., Gasparyan B., Manning C.J., Mark D., 2021. Middle Pleistocene environments, landscapes and tephrostratigraphy of the Armenian Highlands: evidence from Bird Farm 1, Hrazdan Valley. J. Quat. Sci., 37(1): 6-27.

Siebert L., Simkin T., Kimberly P., 2010. Volcanoes of the World. Univ of California Press.

Sorokin V.M., Yanina T.A., Bezrodnykh Yu P., Romanyuk B.F., 2018. Identification and age of submarine Girkanian sediment beds (Upper Pleistocene) in the Caspian Sea. Quat. Int., 465: 152-157. https://doi.org/10.1016/j.quaint.2016.08.044

Stevens T., Buylaert J.P., Thiel C., Újvári G., Yi S., Murray A.S., Frechen M., Lu H., 2018. Ice-volume-forced erosion of the Chinese Loess Plateau global Quaternary stratotype site. Nature communications, 9(1): 1-12. https://doi.org/10.1038/s41467-018-03329-2

Sychev N. V., Konstantinov E. A., Zakharov A. L., Frechen M., Tsukamoto S., 2022. New Data on Geochronology of the Upper Quaternary Loess–Soil Series in the Terek–Kuma Lowland. Lithol Miner Resour 57: 336–347. https://doi.org/10.1134/S0024490222040071

Tesakov A.S., Frolov P.D., Titov V.V., Dickinson M., Meijer T., Parfitt S.A., Preece R.C., Penkman K.E., 2020. Aminostratigraphical test of the East European Mammal Zonation for the late Neogene and Quaternary. Quat. Sci. Rev., 245: 106434. https://doi.org/10.1016/j.quascirev.2020.106434

Timar-Gabor A., Panaiotu C., Vereș D., Necula C., Constantin D., 2017. The lower Danube loess, new age constraints from luminescence dating, magnetic proxies and isochronous tephra markers. In: Landform Dynamics and Evolution in Romania (pp. 679-697). Springer, Cham.

Tolstykh M.L., Naumov V.B., Gurbanov A.G., Gazeev V.M., Bogatikov O.A., Kononkova N.N., 2001. Composition of magmatic melts of Elbrus and Kazbek volcanoes, Caucasus: Evidence from inclusions in minerals. Geochem Int 39(4): 391-397

Trofimov V.T. (Ed.), 2008. Key geological sections of the loess deposits of the Northern Eurasia. M.V. Lomonosov Moscow State University, Geology Department. Moscow: University Book House, 607 p. (Opornye injenerno-geologicheskie razrezy lessovych porod Severnoi Evrazii) [In Russian].

Tsekhovskii Yu.G., Muraviev V.I., Babushkin D.A., 1998. Quaternary volcanic ashes of the Eastern-European Plain. Lihology and Mineral Deposits 3:292–307 [In Russian].

Vakhrameeva, P., Koutsodendris, A., Wulf, S., Portnyagin, M., Appelt, O., Ludwig, T., Trieloff, M. & Pross, J. 2021: Land-sea correlations in the Eastern Mediterranean region over the past c. 800 kyr based on macro- and cryptotephras from ODP Site 964 (Ionian Basin). Quaternary Science Reviews 255, 106811.

Van Baak C.G., Grothe A., Richards K., Stoica M., Aliyeva E., Davies G.R., Kuiper K.F., Krijgsman W., 2019. Flooding of the Caspian Sea at the intensification of Northern Hemisphere Glaciations. Global Planetary Change, 174: 153-163. https://doi.org/10.1016/j.gloplacha.2019.01.007

Velichko A.A., 1990. Loess-paleosol formation on the Russian Plain. Quat. Int., 7: 103-114

Velichko A.A., Catto N.R., Kononov M.Y., Morozova T.D., Novenko E.Y., Panin P.G., Ryskov G.Y., Semenov V.V., Timireva S.N., Titov V.V., Tesakov A.S., 2009. Progressively cooler, drier interglacials in southern Russia through the Quaternary: Evidence from the Sea of Azov region. Quat. Int., 198(1-2): 204-219. https://doi.org/10.1016/j.quaint.2008.06.005

Velichko A.A., Morozova T.D., Borisova O.K., Timireva S.N., Semenov V.V., Kononov Y.M., Titov V.V., Tesakov A.S., Konstantinov E., Kurbanov R.N., 2012. Development of the steppe zone in southern Russia based on the reconstruction from the loess-soil formation in the Don-Azov Region. Doklady Earth Sciences, Vol. 445(2): 999-1002. https://doi.org/10.1134/S1028334X12080107

Velichko A.A., Borisova O.K., Kononov Y.M., Konstantinov E.A., Kurbanov R.N., Morozova T.D., Panin P.G., Semenov V.V., Tesakov A.S., Timireva S.N., Frolov P. D., 2017. Reconstruction of Late Pleistocene events in the periglacial area in the southern part of the East European Plain. Doklady Earth Sciences, Vol. 475(2): 895-899. https://doi.org/10.1134/S1028334X17080098

Velichko A.A. and Morozova T.D., 2010. Basic features of late Pleistocene soil formation in the east European plain and their paleogeographic interpretation. Eurasian Soil Science, 43(13): 1535-1546. https://doi.org/10.1134/S1064229310130120

Veres D., Lane C.S., Timar-Gabor A., Hambach U., Constantin D., Szakács A., Fülling A., Onac B.P., 2013. The Campanian Ignimbrite/Y5 tephra layer–A regional stratigraphic marker for Isotope Stage 3 deposits in the Lower Danube region, Romania. Quat. Int., 293: 22-33.

Wolf D., Baumgart P., Meszner S., Fülling A., Haubold F., Sahakyan L., Meliksetian K., Faust D., 2016. Loess in Armenia–stratigraphic findings and palaeoenvironmental indications. Proceedings of the Geologists' Association, 127(1): 29-39.

Yanina T.A., 2013. Biostratigraphy of the Middle and Upper Pleistocene of the Caspian region. Quat. Int., 284: 85-97. https://doi.org/10.1016/j.quaint.2012.02.008

Yanina T., 2014. The Ponto-Caspian region: Environmental consequences of climate change during the Late Pleistocene. Quat. Int., 345: 88-99. https://doi.org/10.1016/j.quaint.2014.01.045

Yanina T., Sorokin V., Bezrodnykh Yu, Romanyuk B., 2014. The Girkanian epoch in the Pleistocene history of the Caspian Sea. Vestnik Moskovskogo Unviersiteta, Seriya Geografiya, 3, 3-9 [In Russian].

Yanina T., Sorokin V., Bezrodnykh Yu, Romanyuk B., 2018. Late Pleistocene climatic events reflected in the Caspian Sea geological history (based on drilling data). Quat. Int., 465: 130-141. https://doi.org/10.1016/j.quaint.2017.08.003

Yanina T, Bolikhovskaya N, Sorokin V, Romanyuk B, Berdnikova A, Tkach N., 2021. Paleogeography of the Atelian regression in the Caspian Sea (based on drilling data). Quat. Int., 590: 73-84. https://doi.org/10.1016/j.quaint.2020.07.023

Zastrozhnov A., Danukalova G., Shick S., van Kolfshoten T., 2018. State of stratigraphic knowledge of Quaternary deposits in European Russia: Unresolved issues and challenges for further research. Quat. Int., 478, 4-26. https://doi.org/10.1016/j.quaint.2017.03.037

Figure captions

Fig. 1. Location of the study area relative to plate boundaries (a) and tephra sites (b). In a: Volcanoes are shown with triangles: dark purple for active, and pale purple for Pleistocene ones (the data from the Smithsonian's Global Volcanism Program). Elbrus (west) and Kazbek (east) volcanoes considered in this paper are shown with red triangles. Red lines show plate boundaries; green elongated field – Greater Caucasus Range. In **b**: Yellow circles show tephra sites sampled for this study, magenta circles - other sites with geochemically identified tephra from different volcanoes (Pyle et al., 2006; Karátson et al., 2016). Tephra labels (TMG, OTK, TSK, BU, SARM, and VL) are explained in the text; tephra samples near Elbrus volcano are listed in Table S1, and their location is shown in Fig. S1 in the Supplementary Text. Small red circles show the position of the Keli Highland vents.

Fig. 2. a – The two-tipped Elbrus volcano seen from the northeast; **b-g** – selected distal tephras: **b and c** – OTK tephra deposit (b- general view, c- close-up view); **d and e** – TMG tephra deposit (d- general view, note a person left of the label; c- close-up view); **f and g** – TSK tephra deposit (f – general view of the upper part of >10 m thick deposit; g – detail, thickness of the labeled layer of clean ash is ~10 cm; photos courtesy A. Leksin).

Fig. 3. Left: Rank order plots of single-crystal zircon (U-Th)/He data corrected for disequilibrium. Blue horizontal bars correspond to 2 sigma uncertainties for individual analyses; translucent analyses are not included in the weighted mean calculation for the reasons given in Table S8. The thick black or purple vertical lines through each population represent the weighted mean age, the outer dashed horizontal lines mark the corresponding 95% confidence intervals or standard deviation (for sample Elbrus-5-5). Note that for sample Elbrus-5-5 one single eruption age (black bars) or two eruption ages (purple bars) are statistically possible. Right: Rank order plots of zircon U-Th disequilibrium and U-Pb ages; uncertainties are 1 sigma. Full data are listed in Supplementary Tables S2-12.

Fig. 4. Back-scattered electron images of Elbrus tephras. **A** – pumice from TSK tephra; **B** – OTK tephra; **C** - coarse sand matrix from the Elbrus-5-5 proximal tephra (BU?); **D** –TMG; **E** – SARM, **F** –VL. Tephra samples were mounted in epoxy and polished on one side.

Fig. 5. Composition of distal tephra glasses from this study compared to bulk rock compositions of three major Quaternary volcanic centers in the Greater Caucasus as well as to Elbrus and Keli proximal glasses, and to glasses from the ~40 ka old Campanian Ignimbrite ash (CI/Y5) identified in the Kostenki area north of our study sites (Pyle et al.,

2006). Rock compositions are from Tolstych et al., 2001; Gazeev et al., 2004, 2011; Lebedev et al., 2010a; Tutberidze, 2012; Chernyshev et al., 2014; Parfenov et al., 2019; Bewick et al., 2022. Dashed line separates rhyolitic and dacitic fields at Na_2O=5 wt %. Solid lines divide fields of medium-K and high-K rocks following Le Maitre et al. (2002). Oxide contents are given in wt %. Uncertainty of the single point analyses can be estimated from 2 s.d. of reference sample measurements (Supplementary Table S16). Parametrization of the analytical uncertainty depending on element concentrations is presented in Portnyagin et al. (2020).

Fig. 6. Composition of glasses from the individual tephra deposits considered in the text. Uncertainty of the single point analyses can be estimated from 2 s.d. of reference sample measurements (Supplementary Table S16). Parametrization of the analytical uncertainty depending on element concentrations is presented in Portnyagin et al. (2020).

Fig. 7. Variations of selected trace elements in proximal and distal Elbrus tephra glasses in comparison with Quaternary Elbrus lavas and ignimbrites (Lebedev et al., 2010; Chernyshev et al., 2014; Bindeman et al., 2021). Error bars correspond to ±10% for trace elements and ±2 wt % for SiO_2, which are conservative estimates for the LA-ICP-MS data based on repeated standard measurements (2 s.d.; Supplementary Table S17).

Fig. 8. Mantle normalized average compositions of glass shards from distal tephras in comparison with the compositions of proximal glasses (gray field), Elbrus bulk rocks (black field), and average upper continental crust (Rudnick and Gao, 2003). Elbrus rock compositions are after Bindeman et al. (2021). Primitive mantle composition for normalization after McDonough and Sun (1995).

Fig. 9. Sr, Nd, and Pb isotopic compositions of Elbrus tephras in comparison to proximal Elbrus and Kazbek samples of lavas, tephras, and ignimbrites. Literature data for Elbrus is from Chernyshev et al. (2014), Lebedev et al (2010a), and Chugaev et al (2013); for Kazbek - from Parfenov et al. (2019) and Bewick et al. (2022). Uncertainty of the data obtained in this work is similar to or smaller than the symbol sizes.

Fig. 10. Bi-plots showing unique major and trace element composition of the BU glasses among those from the other distal tephras and their similarity with the glasses from the proximal site Elbrus-5, and, partly, with those from sample Elbrus-6-1.

Fig. 11. Variations of B, V, and Rb in SARM, VL, and TSK tephra glasses. Error bars correspond to ±10% for trace elements, which are conservative estimates for the LA-ICP-MS data based on repeated standard measurements (2 s.d.; Supplementary Table S17).

Fig. 12. Comparison of high-Si and low-Si glass shards in SARM and VL tephras. High-Si glasses have SiO_2>76 wt %, low-SiO_2 glasses <73 wt %. The group of high-Si SARM glasses includes glass shards with moderately high Y content (~10 ppm), low-Y high-Si glasses are not included.

Fig. 13. Schematic graphic presentation of the activity from the Elbrus volcanic center during the last 1 Ma. Left column: earlier known activity reconstructed by dating lavas and welded tuffs is shown according to Table 6 in Chernyshev et al. (2014); right column: violent pumice eruptions reconstructed by dating distal and proximal tephras (our results). Numbers left of the eruptions/active periods show respective ages (ka).

Table 1. Distal tephras attributed to the Elbrus volcanic center

E-Supplement

Supplementary Text. Samples and Methods

Supplementary Table S1. Tephra samples used in this research

Supplementary Table S2. (U-Th)/He data

Supplementary Table S3. LA-ICP-MS zircon U-Th disequilibrium geochronology data

Supplementary Table S4. LA-ICP-MS operating parameters used for zircon U-Th disequilibrium geochronology

Supplementary Table S5. Activity ratios of standards used for zircon U-Th disequilibrium geochronology

Supplementary Table S6. Parameters setting for zircon U-Th disequilibrium dating by SIMS

Supplementary Table S7. SIMS zircon U-Th disequilibrium geochronology data

Supplementary Table S8. SIMS zircon U-Pb geochronology data

Supplementary Table S9. LA-MC-ICP-MS operating parameters used for zircon U-Pb geochronology

Supplementary Table S10. LA-MC-ICPMS U-Pb datatable for zircon grains from the Gizel-2-1 sample

Supplementary Table S11. TuffZirc age for Elbrus-5-5

Supplementary Table S12. Deconvolution of (U-Th)/He dates for sample Elbrus 5-5

Supplementary Tables S13-15. Major element composition of glasses from distal and proximal tephras considered in this study

Supplementary Table S16. Electron microprobe data on reference materials

Supplementary Table S17. LA-ICP-MS single glass shard data for Elbrus tephra samples and reference materials

Supplementary Table S18. Sr-Nd-Pb isotope compositions for Elbrus proximal and distal samples

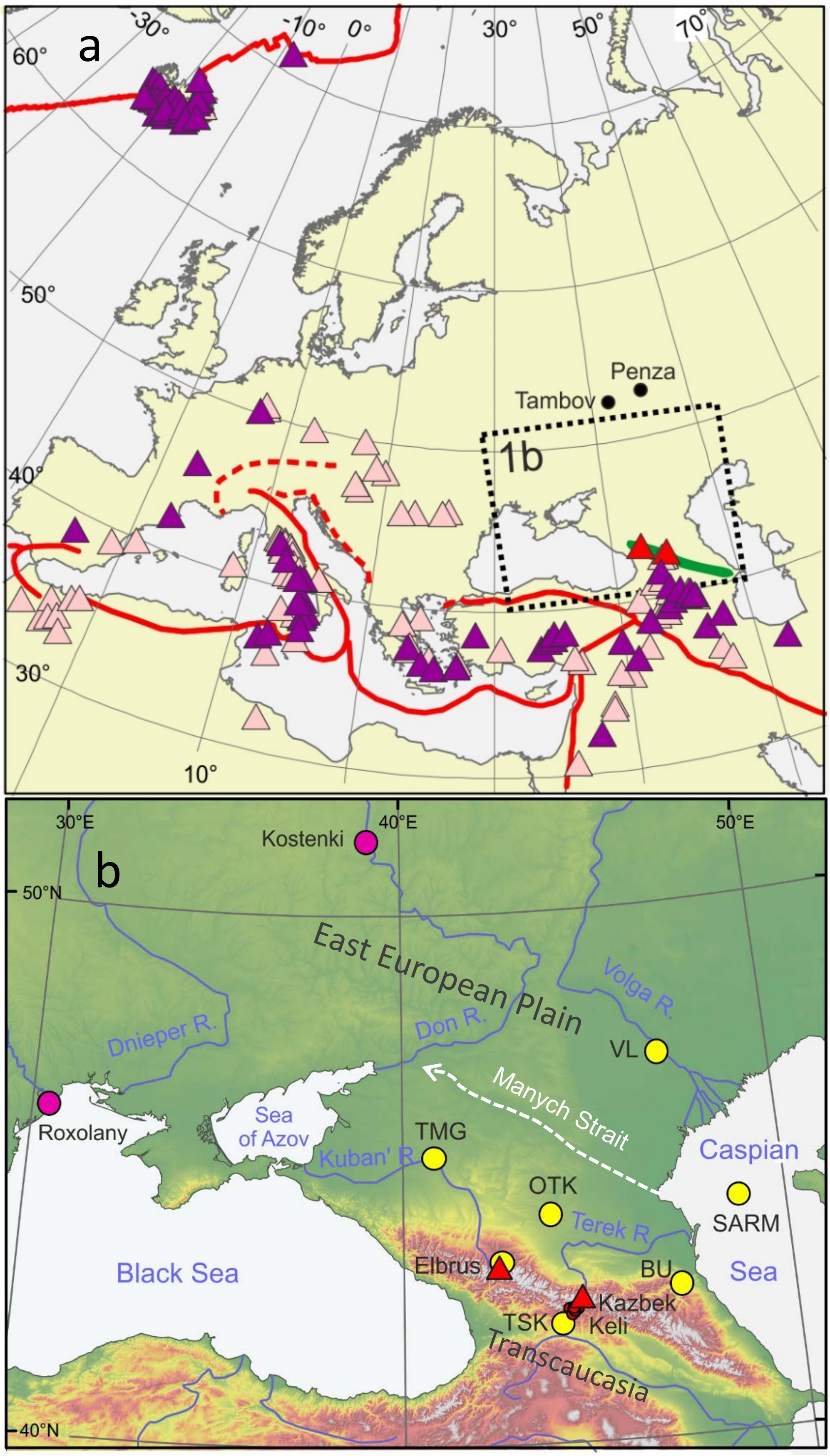
a
-30°
-10°
0°
30°
50°
70°
60°
50°
40°
30°
10°
Tambov
Penza
1b
b
30°E
40°E
50°E
50°N
40°N
Kostenki
East European Plain
Volga R.
Dnieper R.
Don R.
VL
Manych Strait
Roxolany
Sea of Azov
TMG
Kuban' R.
Caspian
SARM
OTK
Terek R.
Black Sea
Elbrus
BU
Sea
Kazbek
TSK
Keli
Transcaucasia

Fig. 1

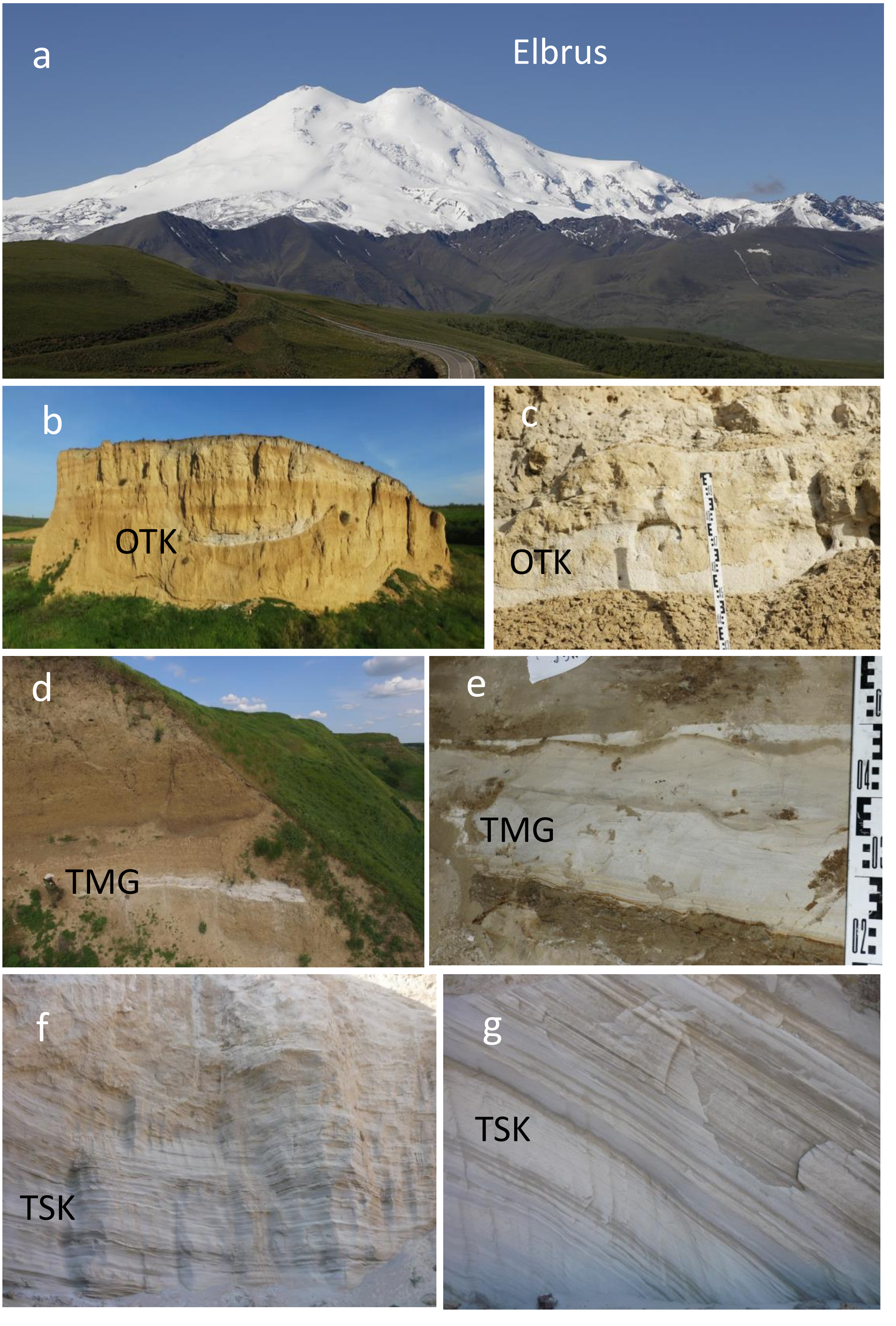

Fig. 2

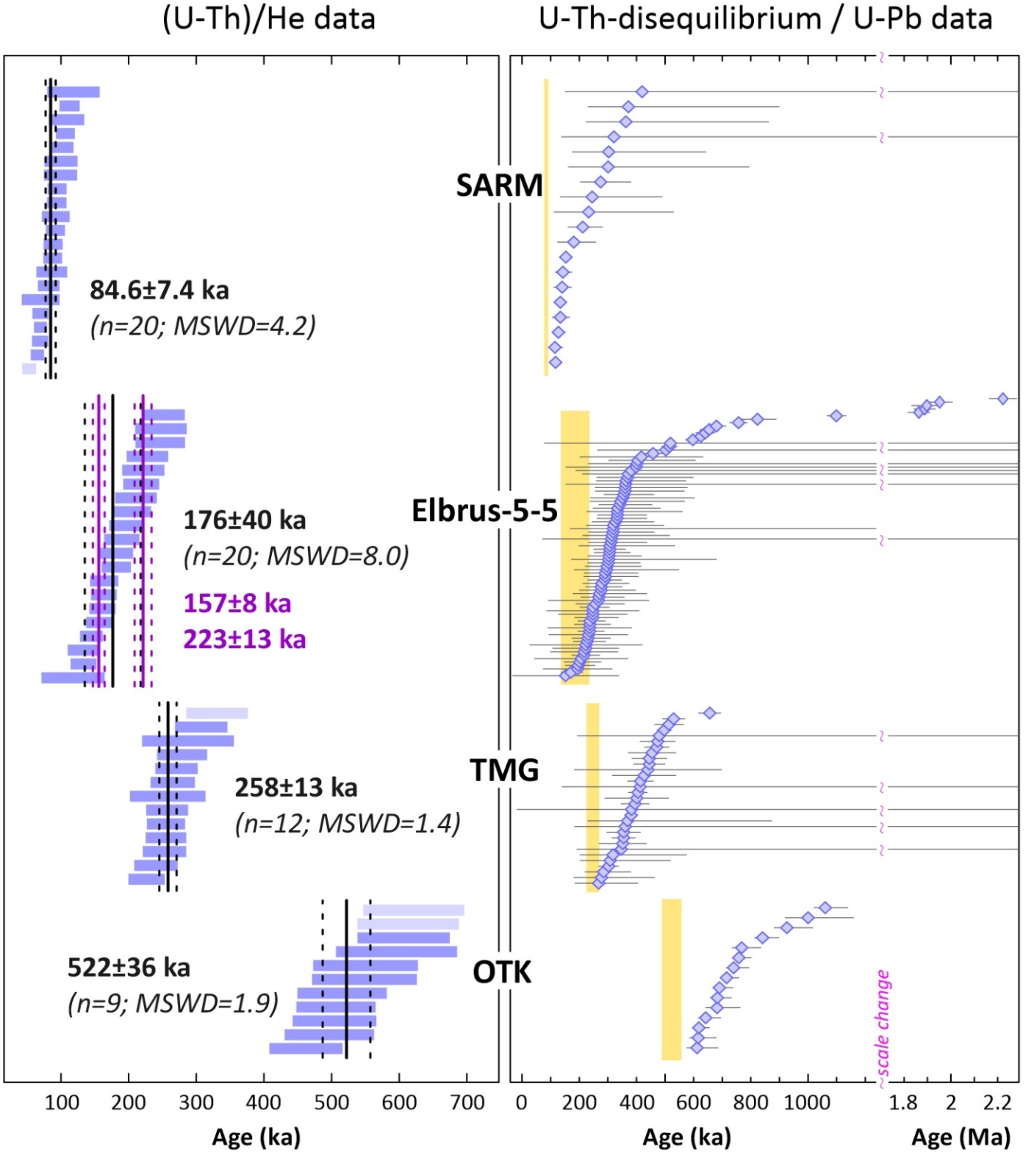

(U-Th)/He data
U-Th-disequilibrium / U-Pb data
SARM
84.6±7.4 ka
(n=20; MSWD=4.2)
Elbrus-5-5
176±40 ka
(n=20; MSWD=8.0)
157±8 ka
223±13 ka
TMG
258±13 ka
(n=12; MSWD=1.4)
OTK
522±36 ka
(n=9; MSWD=1.9)
scale change
100
200
300
400
500
600
700
Age (ka)
0
200
400
600
800
1000
1.8
2
2.2
Age (ka)
Age (Ma)

Fig. 3

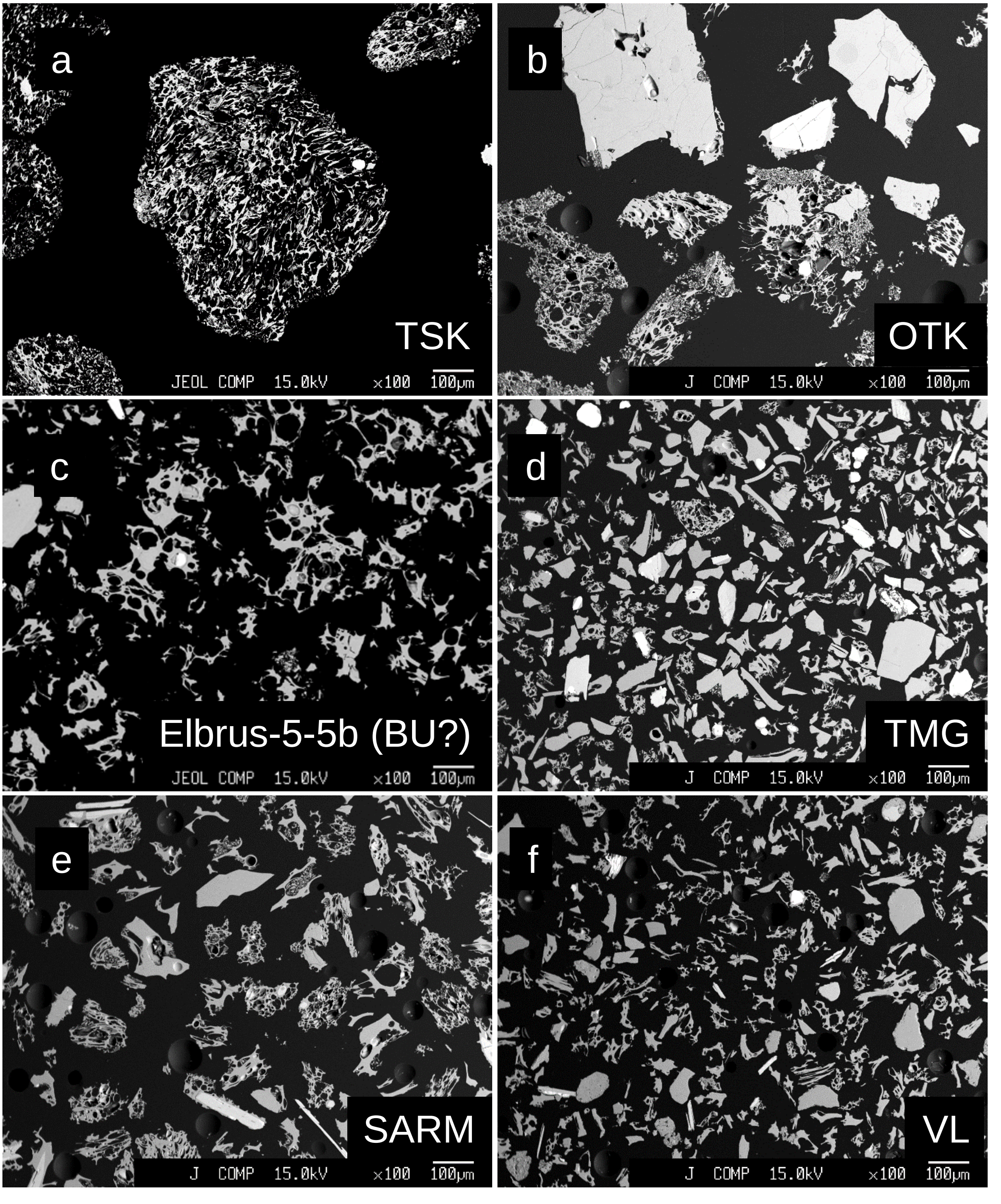
a
TSK
JEOL COMP 15.0kV ×100 100μm
b
OTK
J COMP 15.0kV ×100 100μm
c
Elbrus-5-5b (BU?)
JEOL COMP 15.0kV ×100 100μm
d
TMG
J COMP 15.0kV ×100 100μm
e
SARM
J COMP 15.0kV ×100 100μm
f
VL
J COMP 15.0kV ×100 100μm

Fig. 4

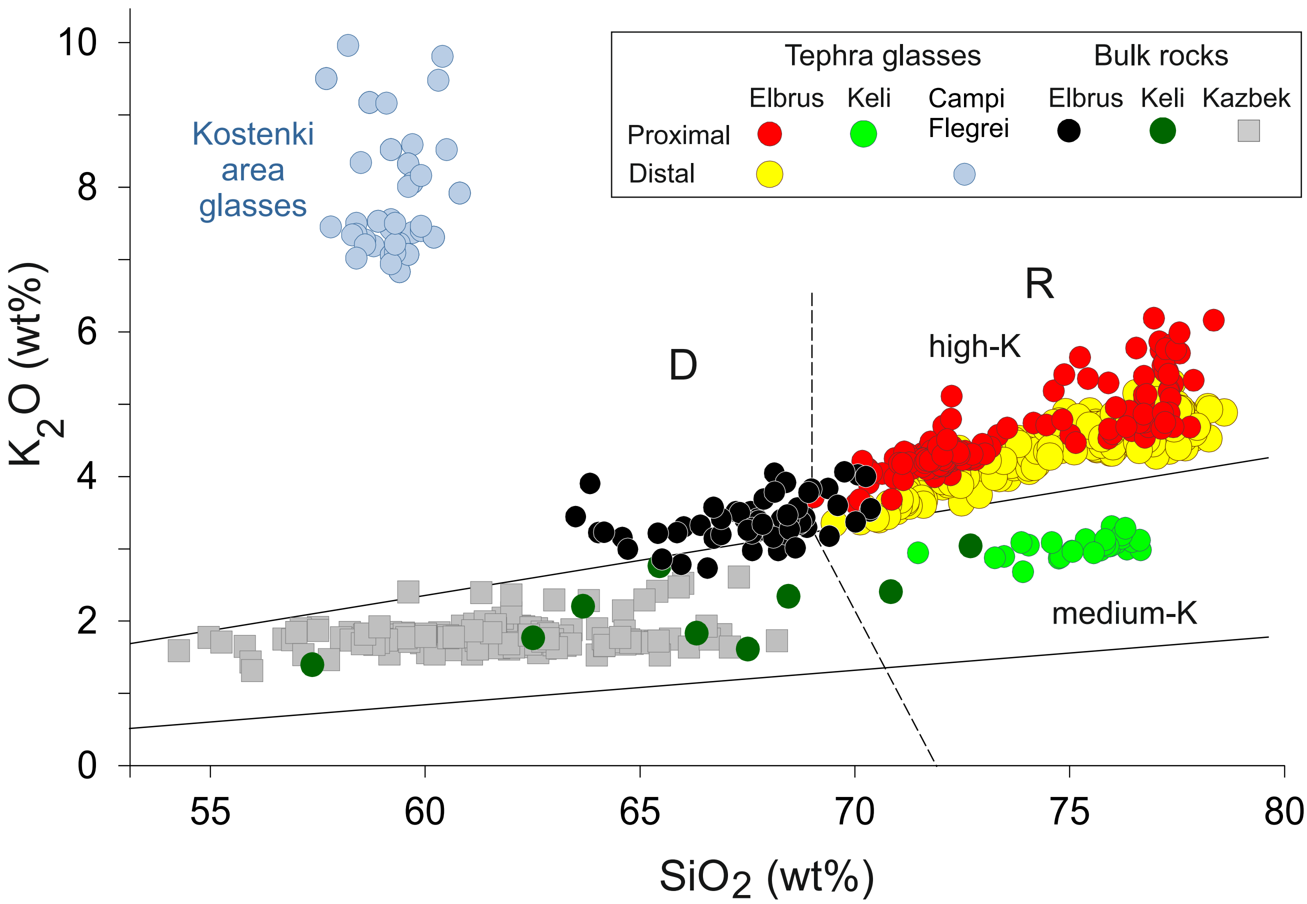

Tephra glasses
Bulk rocks
Elbrus
Keli
Campi Flegrei
Elbrus
Keli
Kazbek
Proximal
Distal
Kostenki area glasses
R
D
high-K
medium-K
K_2O (wt%)
SiO_2 (wt%)
0
2
4
6
8
10
55
60
65
70
75
80

Fig. 5

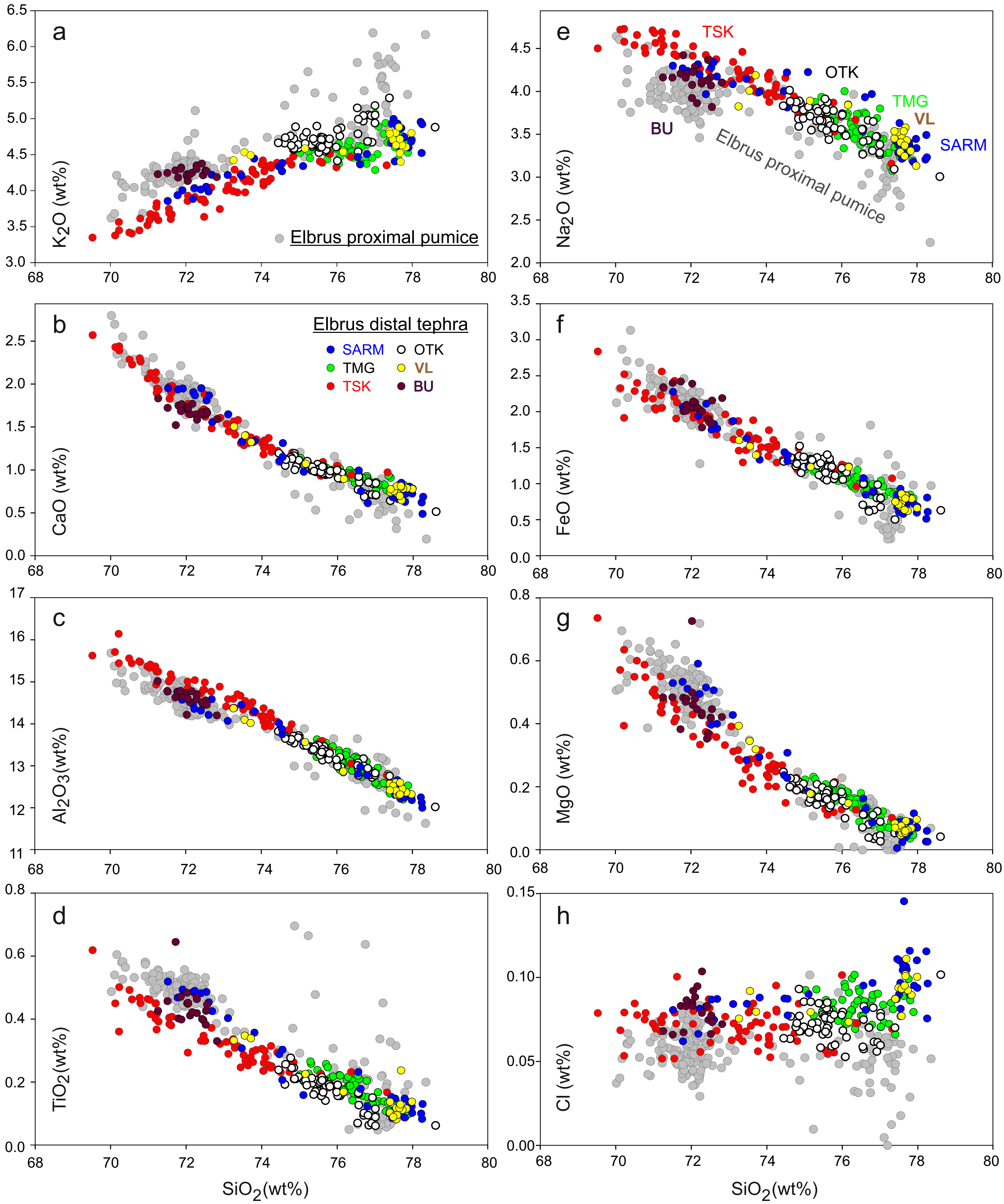

a
b
c
d
e
f
g
h
K2O (wt%)
CaO (wt%)
Al2O3(wt%)
TiO2(wt%)
Na2O (wt%)
FeO (wt%)
MgO (wt%)
Cl (wt%)
SiO2(wt%)
SiO2(wt%)
Elbrus proximal pumice
Elbrus distal tephra
SARM
OTK
TMG
VL
TSK
BU
Elbrus proximal pumice

Fig. 6

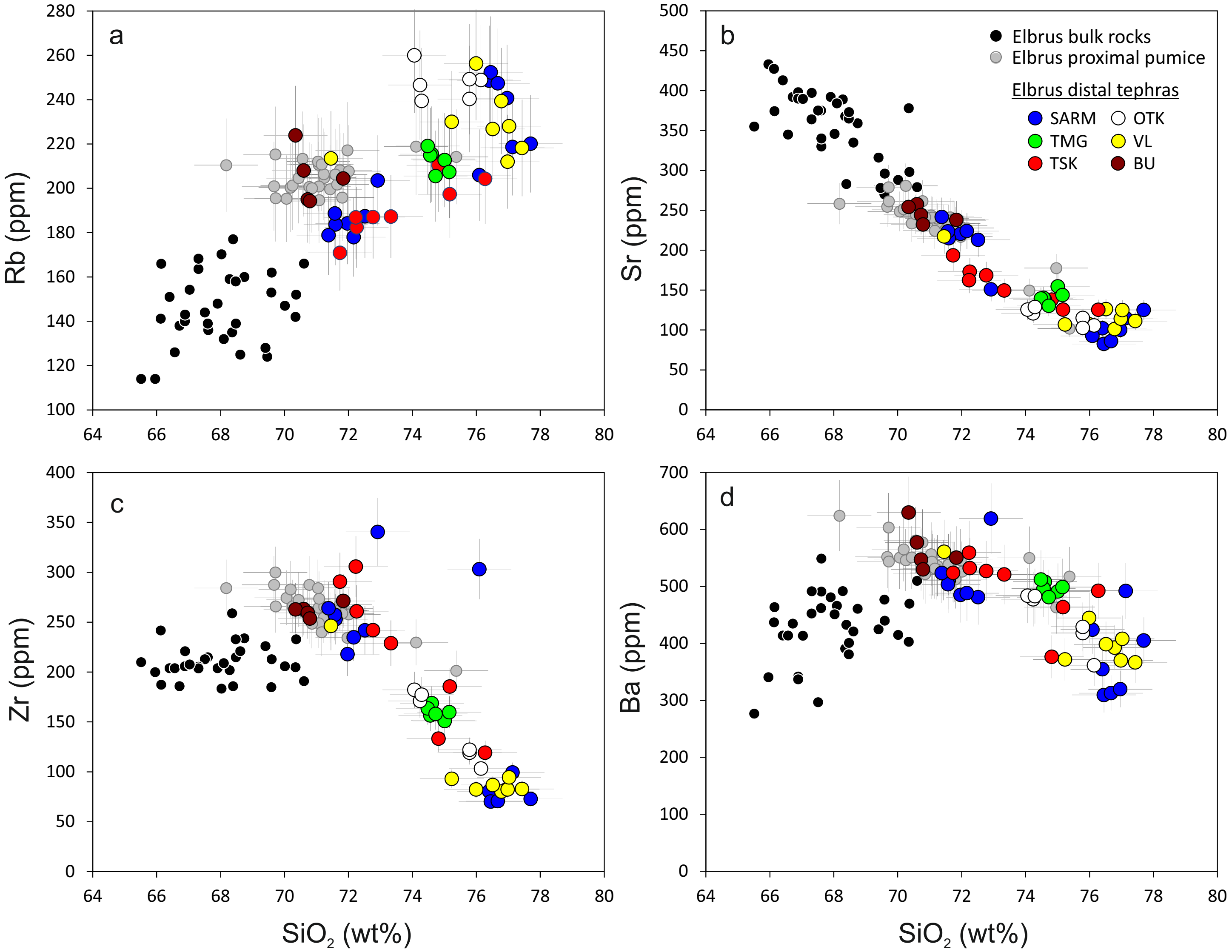

a
b
c
d
Rb (ppm)
Sr (ppm)
Zr (ppm)
Ba (ppm)
SiO2 (wt%)
SiO2 (wt%)
Elbrus bulk rocks
Elbrus proximal pumice
Elbrus distal tephras
SARM
OTK
TMG
VL
TSK
BU

Fig. 7

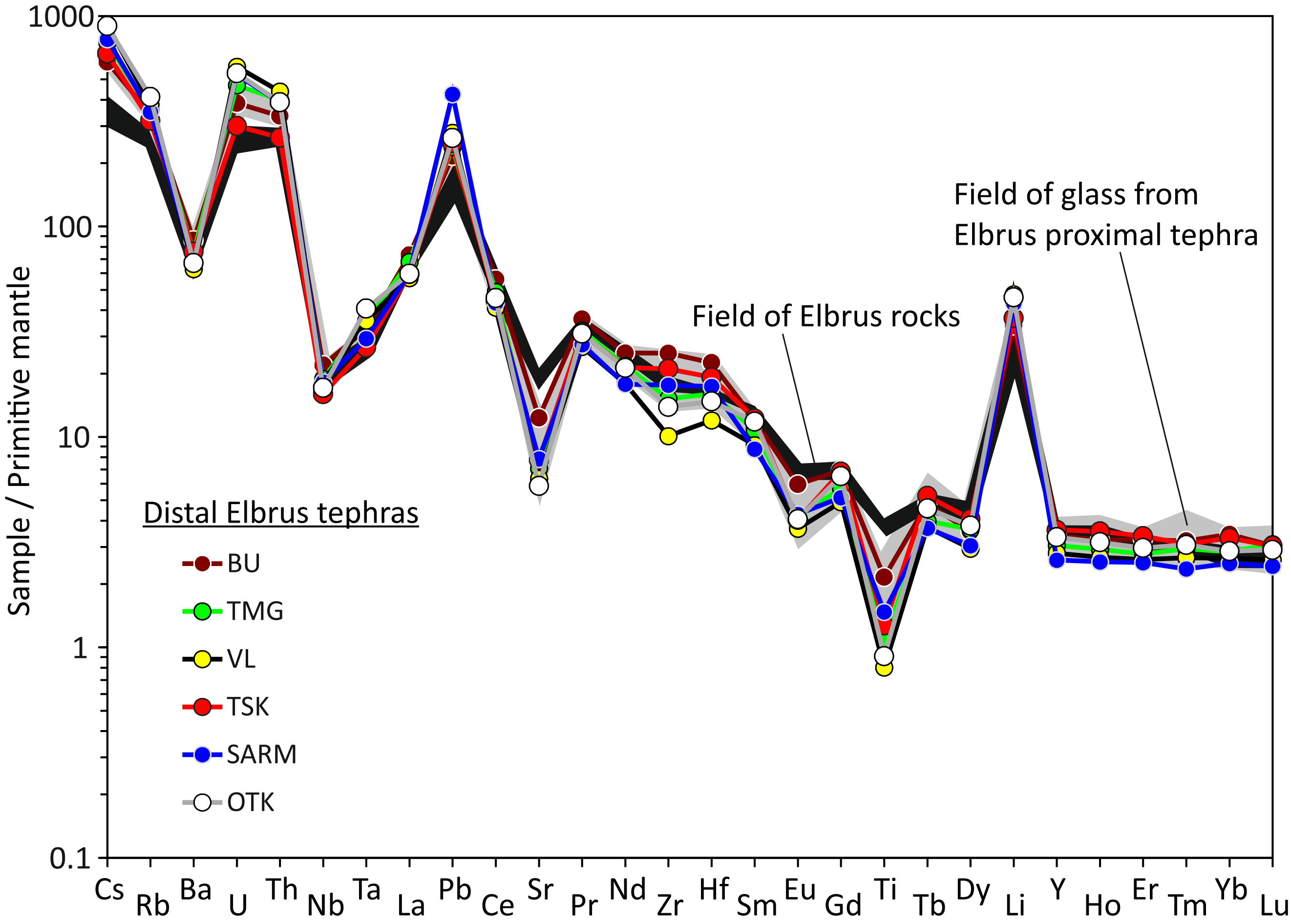
1000
100
10
1
0.1
Sample / Primitive mantle
Cs
Rb
Ba
U
Th
Nb
Ta
La
Pb
Ce
Sr
Pr
Nd
Zr
Hf
Sm
Eu
Gd
Ti
Tb
Dy
Li
Y
Ho
Er
Tm
Yb
Lu
Field of glass from
Elbrus proximal tephra
Field of Elbrus rocks
Distal Elbrus tephras
BU
TMG
VL
TSK
SARM
OTK

Fig. 8

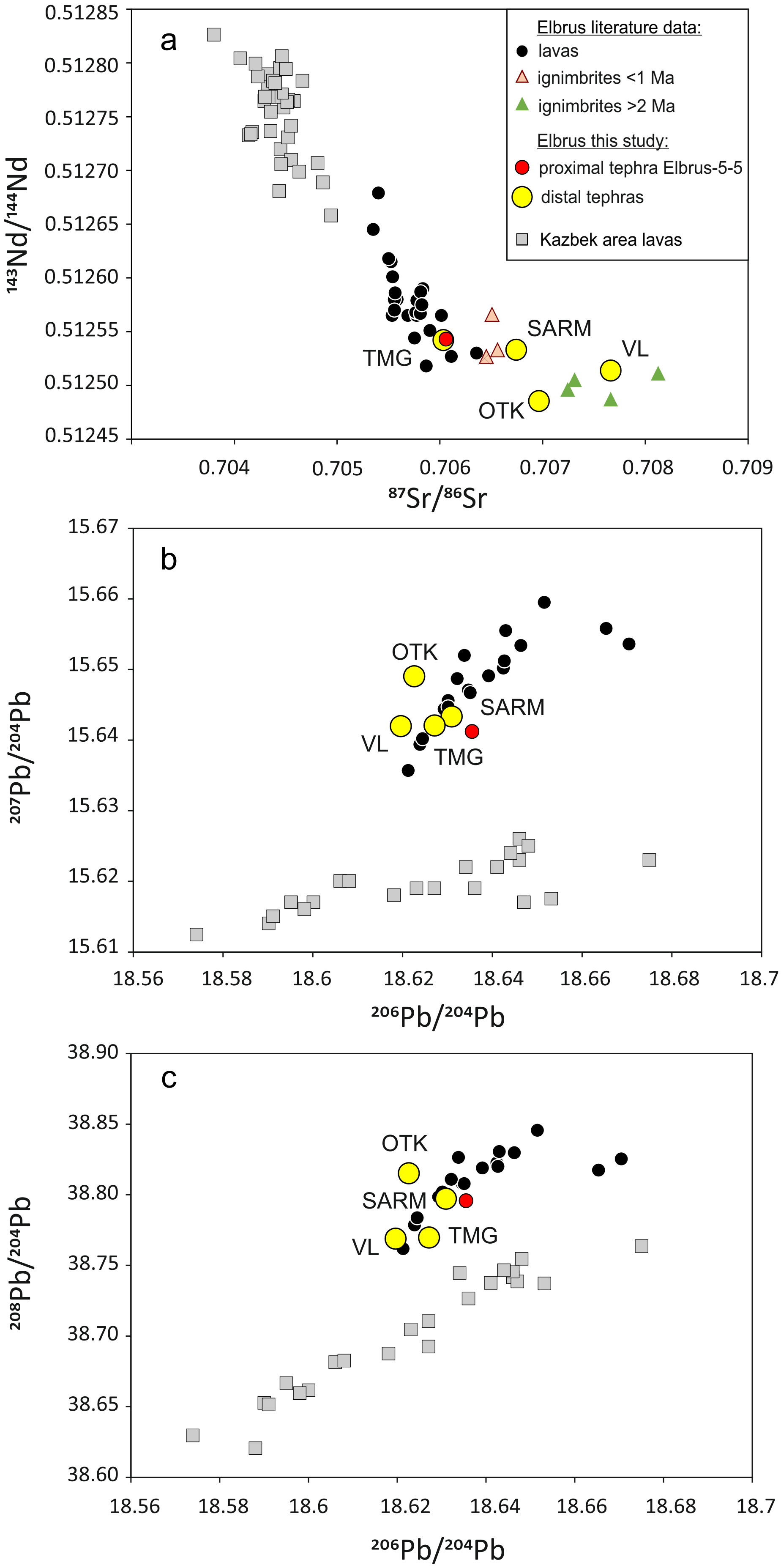
a
b
c
Elbrus literature data:
lavas
ignimbrites <1 Ma
ignimbrites >2 Ma
Elbrus this study:
proximal tephra Elbrus-5-5
distal tephras
Kazbek area lavas
SARM
VL
TMG
OTK
143Nd/144Nd
87Sr/86Sr
207Pb/204Pb
206Pb/204Pb
208Pb/204Pb
0.51285
0.51280
0.51275
0.51270
0.51265
0.51260
0.51255
0.51250
0.51245
0.704
0.705
0.706
0.707
0.708
0.709
15.67
15.66
15.65
15.64
15.63
15.62
15.61
38.90
38.85
38.80
38.75
38.70
38.65
38.60
18.56
18.58
18.6
18.62
18.64
18.66
18.68
18.7

Fig. 9

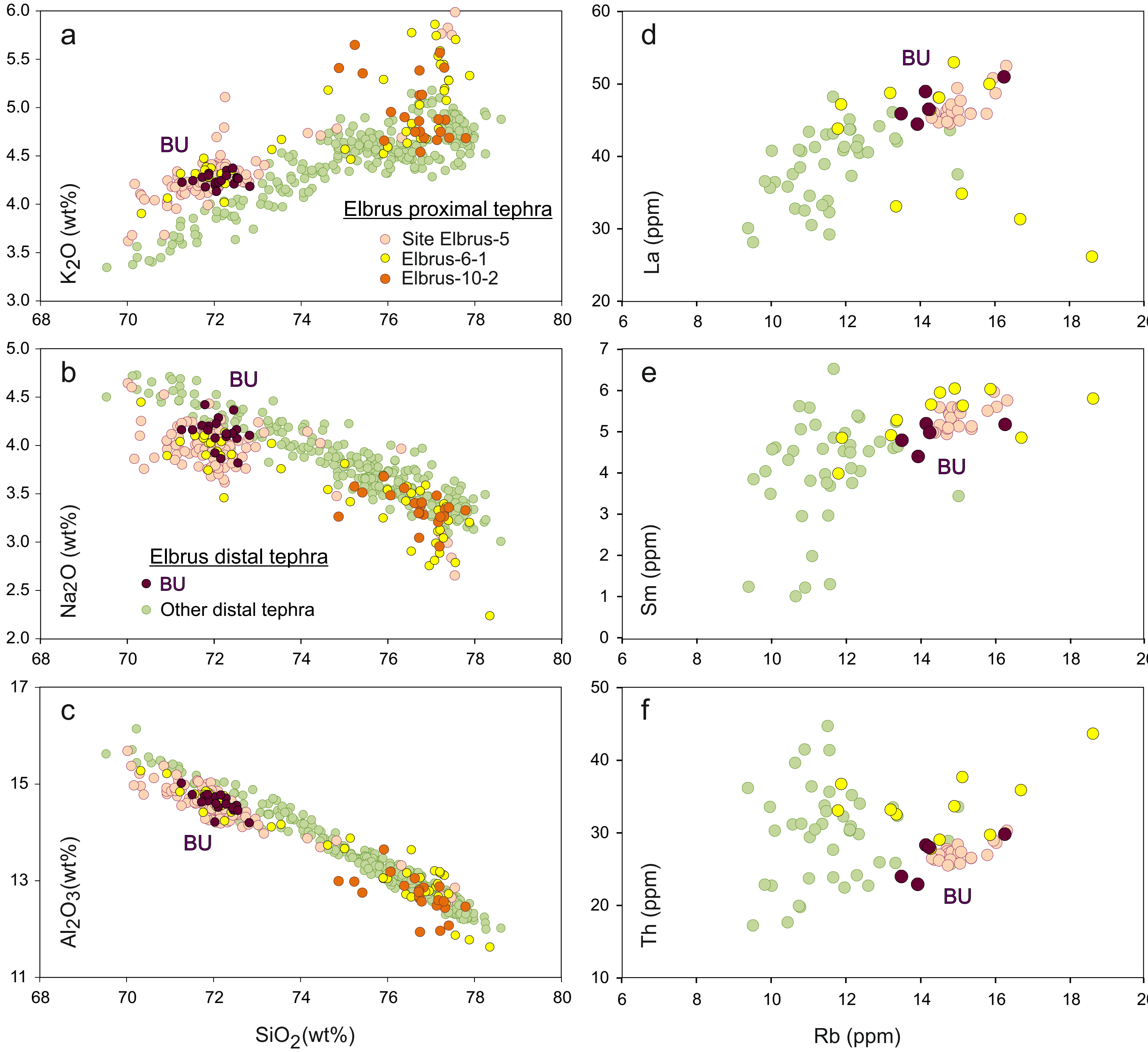
a
BU
Elbrus proximal tephra
Site Elbrus-5
Elbrus-6-1
Elbrus-10-2
K2O (wt%)
b
BU
Elbrus distal tephra
BU
Other distal tephra
Na2O (wt%)
c
BU
Al2O3(wt%)
SiO2(wt%)
d
BU
La (ppm)
e
BU
Sm (ppm)
f
BU
Th (ppm)
Rb (ppm)

Fig. 10

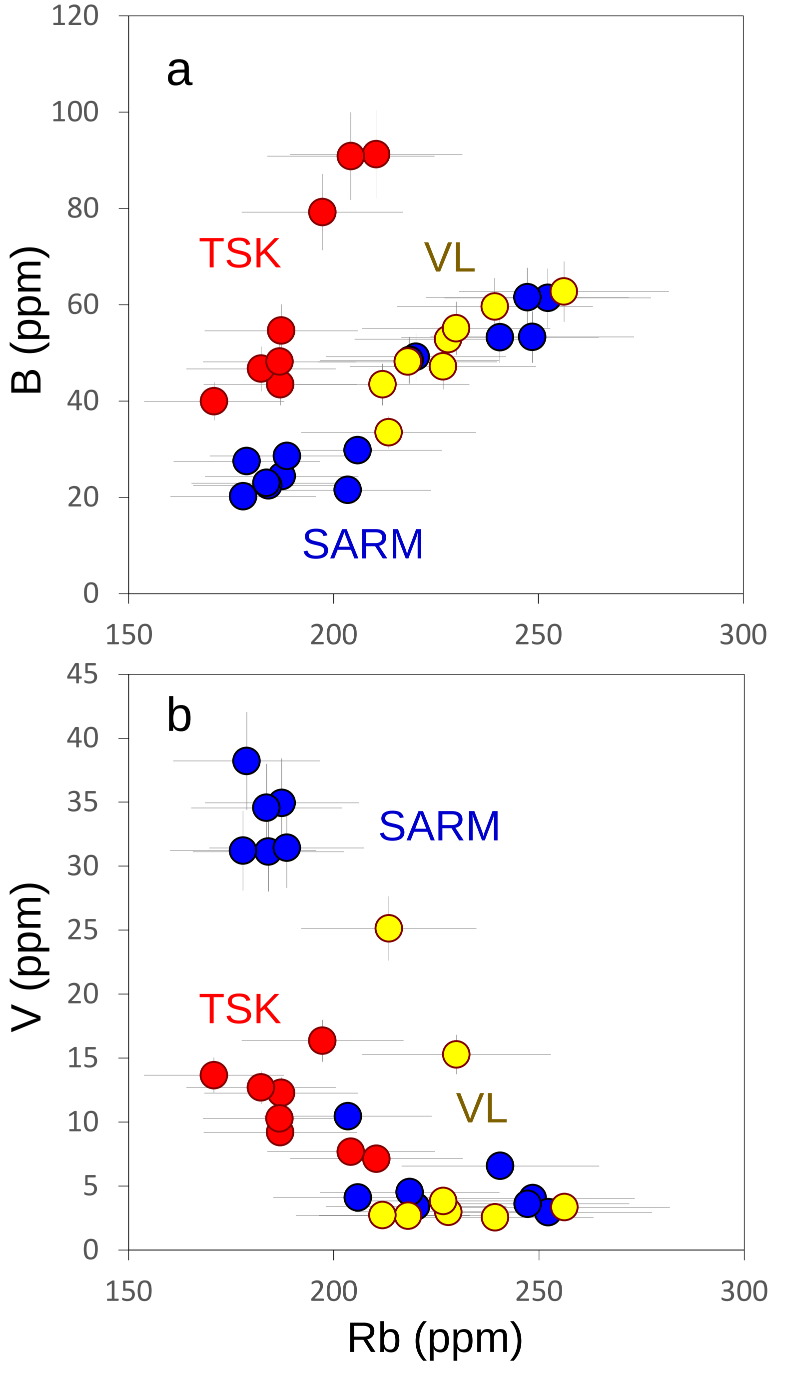

Fig. 11

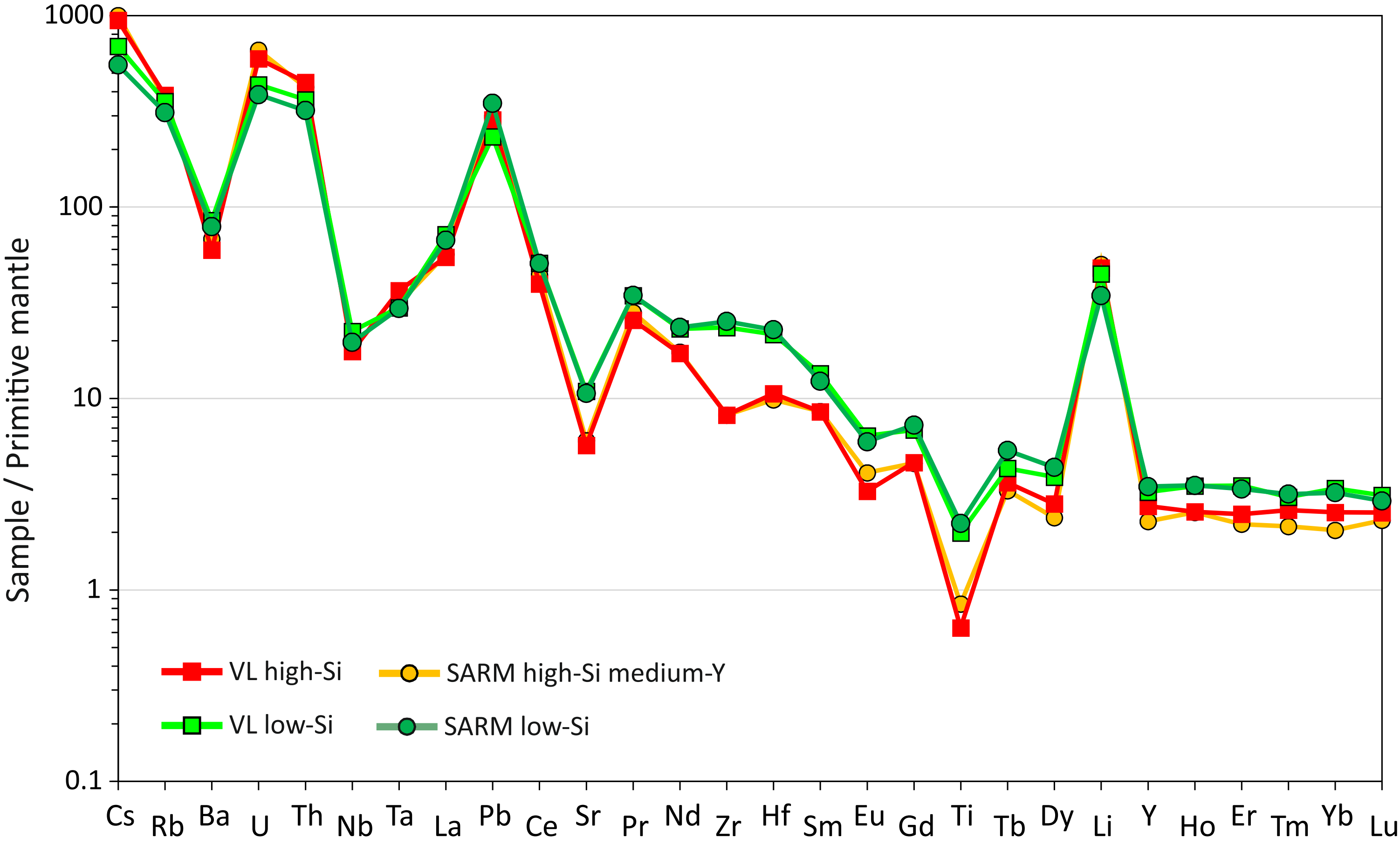

Sample / Primitive mantle
1000
100
10
1
0.1
Cs
Rb
Ba
U
Th
Nb
Ta
La
Pb
Ce
Sr
Pr
Nd
Zr
Hf
Sm
Eu
Gd
Ti
Tb
Dy
Li
Y
Ho
Er
Tm
Yb
Lu
VL high-Si
SARM high-Si medium-Y
VL low-Si
SARM low-Si

Fig. 12

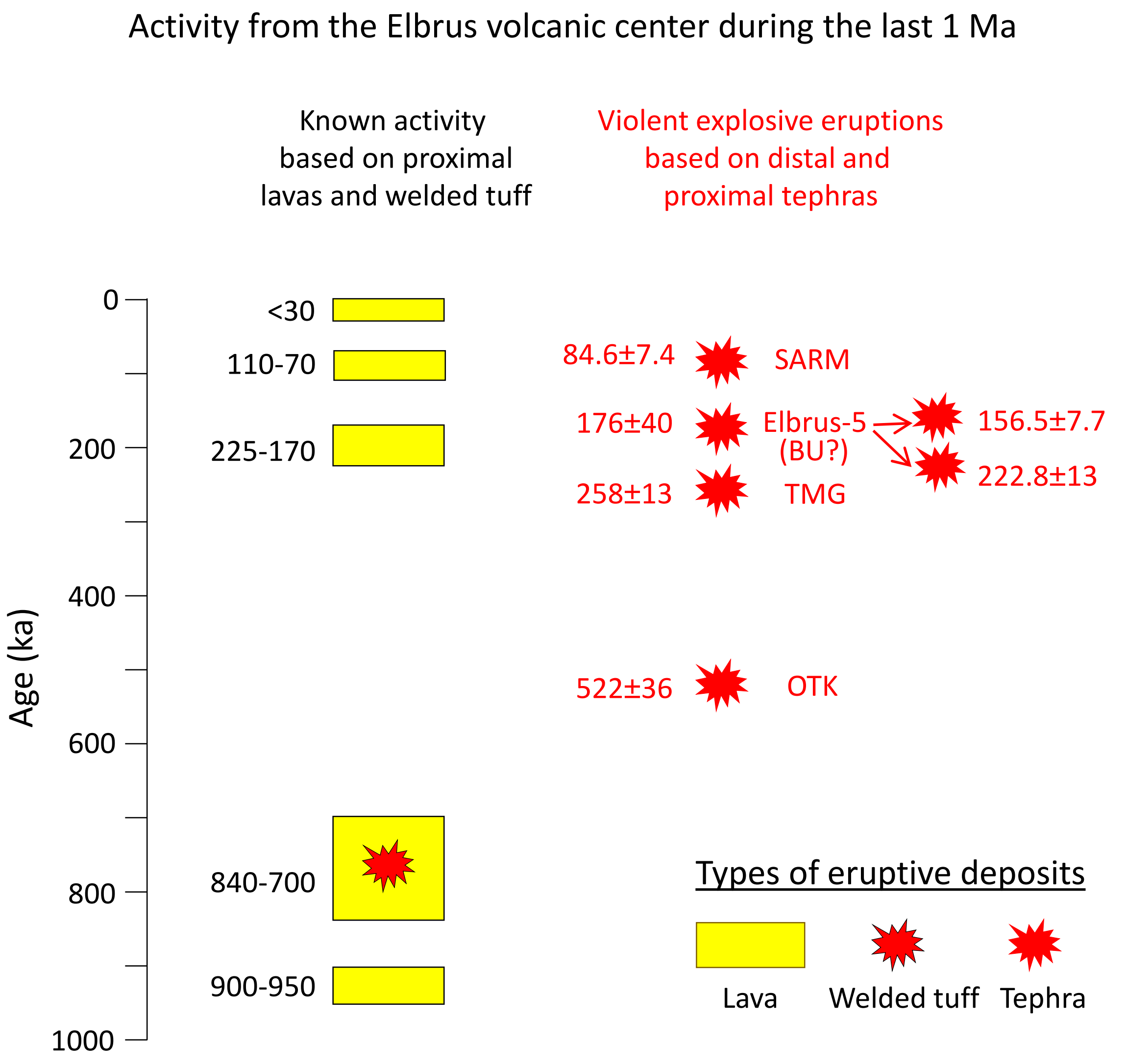
Activity from the Elbrus volcanic center during the last 1 Ma
Known activity based on proximal lavas and welded tuff
Violent explosive eruptions based on distal and proximal tephras
Age (ka)
0
200
400
600
800
1000
<30
110-70
225-170
840-700
900-950
84.6±7.4
SARM
176±40
Elbrus-5 (BU?)
156.5±7.7
222.8±13
258±13
TMG
522±36
OTK
Types of eruptive deposits
Lava
Welded tuff
Tephra

Fig. 13

Table 1. Distal tephras attributed to the Elbrus volcanic center

Tephra deposit label	Tephra location	Coordinates	Description and stratigraphic position	Dated sample	ZDD eruption age ± 95% conf. int. (ka)*	Crystallization age (ka)	Previous age estimate (ka)	Decription/ previous age reference
SARM	Caspian Sea core	N 44.36303° E 48.79609°	0.75 m thick layer of fine ash in the deposits of the Hyrcanian transgression	SARM-4	84.6 ± 7.4	115 – >350**	~80	Sorokin et al., 2018***
VL likely correlates to SARM	Lower streams of *Volga R.*, near Vladimirovka village	N 47.17943° E 47.03740°	0.7 m thick and 100 m long lens of very fine ash in the deposits of the Late Khazarian transgression	-	-	-	~100	Lavrushin at al., 1998
TSK	*Malaya Liakhva R.*, South Ossetia	N 42.23541° E 44.01675°	>10 m thick redeposited laminated fine to coarse ash, original thickness is not known	-	-	-	-	Gazeev et al., 2011
BU correlates to proximal pumice Elbrus-5-5	Road cut near Buynaksk town, Dagestan	N 42.827739° E 47.077253°	0.15 m thick layer of fine ash within the loess overlying fluvial gravels	Elbrus-5-5	176 ± 40*	171 – 2200	-	Matsapulin et al., 2008
TMG	*Kuban' R.*, near Temizhbekskaia village	N 45.43177° E 40.84137°	0.2-1.5 m thick layered fine ash in a loess-soil sequence; original tephra thickness is likely 0.05 m	TMG	258±13	268 – 656	~20	Melekestsev et al., 2005
OTK	*Kuma R.*, Otkaznensky reservoir	N 44.29480° E 43.85719°	0.7 m thick lens of fine ash to small lapilli in a loess-soil sequence; bottom 0.3 m likely represent non-disturbed ash layer	OTK-3	522 ± 36	612 – 1060	~660	Bolikhovskaya, 1995

Notes:

* The uncertainty for sample Elbrus-5-5 is reported as one standard deviation to honor the fact that the population is over-dispersed.

** Sample SARM was analyzed only by U-Th method revealing some crystal in secular equilibrium and without additional U-Pb data the crystallization age can be constrained to >350 ka.

*** The SARM tephra has not been described earlier, so we present the previously suggested age for the enclosing Hyrcanian deposits.

For the complete list of distal and proximal samples used in this research, see Table S1 and Supplementary Text.